



HAL
open science

Transient nicotine exposure in early adolescent male mice freezes their dopamine circuits in an immature state

Lauren Reynolds, Aylin Gulmez, Sophie Fayad, Renan Costa Campos, Daiana Rigoni, Claire Nguyen, Tinaïg Le Borgne, Thomas Topilko, Domitille Rajot, Clara Franco, et al.

► To cite this version:

Lauren Reynolds, Aylin Gulmez, Sophie Fayad, Renan Costa Campos, Daiana Rigoni, et al.. Transient nicotine exposure in early adolescent male mice freezes their dopamine circuits in an immature state. Nature Communications, 2024, 15 (1), pp.9017. 10.1038/s41467-024-53327-w . hal-04758404

HAL Id: hal-04758404

<https://hal.science/hal-04758404v1>

Submitted on 29 Oct 2024

HAL is a multi-disciplinary open access archive for the deposit and dissemination of scientific research documents, whether they are published or not. The documents may come from teaching and research institutions in France or abroad, or from public or private research centers.

L'archive ouverte pluridisciplinaire **HAL**, est destinée au dépôt et à la diffusion de documents scientifiques de niveau recherche, publiés ou non, émanant des établissements d'enseignement et de recherche français ou étrangers, des laboratoires publics ou privés.

Transient nicotine exposure in early adolescent male mice freezes their dopamine circuits in an immature state

Received: 10 January 2024

Accepted: 8 October 2024

Published online: 18 October 2024

 Check for updates

Lauren M. Reynolds ^{1,2} ✉, Aylin Gulmez¹, Sophie L. Fayad^{1,2}, Renan Costa Campos ³, Daiana Rigoni ³, Claire Nguyen ², Tinaïg Le Borgne ^{1,2}, Thomas Topilko⁴, Domitille Rajot⁴, Clara Franco ², Sebastian P. Fernandez³, Fabio Marti ^{1,2}, Nicolas Heck ², Alexandre Mourot ^{1,2}, Nicolas Renier ⁴, Jacques Barik ³ & Philippe Faure ^{1,2} ✉

How nicotine acts on developing neurocircuitry in adolescence to promote later addiction vulnerability remains largely unknown, but may hold the key for informing more effective intervention efforts. We found transient nicotine exposure in early adolescent (PND 21–28) male mice was sufficient to produce a marked vulnerability to nicotine in adulthood (PND 60+), associated with disrupted functional connectivity in dopaminergic circuits. These mice showed persistent adolescent-like behavioral and physiological responses to nicotine, suggesting that nicotine exposure in adolescence prolongs an immature, imbalanced state in the function of these circuits. Chemogenetically resetting the balance between the underlying dopamine circuits unmasked the mature behavioral response to acute nicotine in adolescent-exposed mice. Together, our results suggest that the perseverance of a developmental imbalance between dopamine pathways may alter vulnerability profiles for later dopamine-dependent psychopathologies.

Smoking is a major contributor to disease burden worldwide, driven by addiction to nicotine¹. The prognosis is particularly bleak for the up to 90% of adult smokers who began in adolescence², as early onset drug use is associated with an elevated risk of addiction throughout the lifetime³. Indeed, epidemiological studies associate adolescent nicotine use with increased risk of not only longer and heavier smoking careers⁴, but also with the development of anxiety disorders and depression^{5,6}, and with the problematic consumption of other drugs, such as alcohol⁴. Studies in animal models have focused to date largely on the differences in the rewarding effects of nicotine in adolescent vs adult rats and mice and on how adolescent nicotine exposure can influence later measures of nicotine reward^{7,8}, but less is known about

how nicotine impacts the adolescent development of neural circuitry to produce these enduring outcomes.

Mature cognitive, emotional, and motivational behaviors emerge across adolescence in parallel to the development of their underlying neurocircuitry. Dopamine (DA) circuitry, in particular, is increasingly considered as a “plasticity system” where its structure and function is shaped by experience during development, creating adaptive behavioral profiles that can endure throughout the lifetime^{9,10}. While this window may allow for performance optimization in the context of a specific environment, it also likely demarcates a period of increased vulnerability to environmental insult¹¹. Nicotine acts directly on DA neurons through its action on nAChRs¹², a family of pentameric

¹Plasticité du Cerveau CNRS UMR8249, École supérieure de physique et de chimie industrielles de la Ville de Paris (ESPCI Paris), Paris, France. ²Neuroscience Paris Seine CNRS UMR 8246 INSERM U1130, Institut de Biologie Paris Seine, Sorbonne Université, Paris, France. ³Université Côte d’Azur, Nice 06560, France; Institut de Pharmacologie Moléculaire & Cellulaire, CNRS, UMR7275 Valbonne, France. ⁴Laboratoire de Plasticité Structurale INSERM U1127, CNRS UMR7225, Sorbonne Université, ICM Institut du Cerveau et de la Moelle Epinière, Paris, France. ✉ e-mail: laurenreynoldsm@gmail.com; phfaure@gmail.com

ligand-gated ion channels. While the effects of nicotine on DA neurons are best studied in adult animals^{13–15}, some evidence does suggest that both the immediate and enduring effects of nicotine on ventral tegmental area (VTA) DA neurons differ between adolescent and adult administration^{16,17}. However, these studies treat DA neurons as a single, homogenous population; whereas VTA DA neurons are increasingly recognized to belong to anatomically distinct circuits, to possess diverse molecular signatures, and to differ in their responses to external stimuli^{18–22}. Indeed, nicotine simultaneously produces both reinforcing and anxiogenic behavioral effects^{23,24}, which rely on distinct DA pathways: the activation of DA neurons projecting to the nucleus accumbens (NAc) produces reinforcement, whereas the inhibition of amygdala (AMG)-projecting DA neurons produces anxiety-like behavior²³. Dopaminergic axons are still connecting to forebrain targets in adolescence¹¹, and are sensitive to disruption by other psychostimulant drugs of abuse²⁵; however whether and how nicotine may alter the development of distinct DA circuits in adolescence to drive later addiction vulnerability remains unknown. Here, we found that male mice exposed to nicotine during early adolescence showed persistent behavioral and electrophysiological markers of vulnerability to nicotine re-exposure as adults, which was associated with a restructuring of dopaminergic functional connectivity as to create an imbalance in VTA-NAc and VTA-AMG signaling. Interestingly, the behavioral and electrophysiological responses to nicotine in these adult mice exposed to nicotine as adolescents closely resembled the phenotype of naïve adolescent mice, suggesting this signaling imbalance is a marker of immaturity in dopaminergic circuits. Finally, we show that chemogenetically resetting an adult-like balance in dopamine signaling in response to nicotine restores a mature behavioral response in adolescent-exposed mice, causally implicating the development of this pathway in a type of naturally occurring resilience to nicotine use that develops in unexposed adults.

Results

Exposure to nicotine during adolescence, but not during adulthood, enduringly increases vulnerability to nicotine use

To model nicotine exposure in the period when human adolescents are most likely to start smoking or using e-cigarettes^{26,27}, we focused on comparing exposure to nicotine early in adolescence in mice (-PND21 – PND 28)¹¹ with exposure in adulthood (>PND60). To this end, male mice underwent a one-week exposure to nicotine (NIC, 100 µg/ml in 2% saccharin) or to 2% saccharin only (SAC) in their home cage drinking bottle either in early adolescence or in adulthood. All mice were tested for sucrose and nicotine consumption five weeks later in a continuous-access free-choice oral self-administration paradigm (Fig. 1A). Mouse weight stayed stable over the course of the task (Supplementary Fig. 1A), and their drinking behavior followed their diurnal behavioral profile, with the greatest drinking volumes shortly after the beginning of the dark cycle, regardless of the solution presented (Supplementary Fig. 1B). All mice showed a strong, dose-dependent preference for the sucrose-containing solution over water (Fig. 1B *left*, 1C *left*, Table 1A, C), with similar overall volumes of liquid consumed (Supplementary Fig. 1C, D), regardless of their pretreatment solution or age.

While rodents, and mice in particular, do not acquire intra-venous self-administration of nicotine as readily as with other stimulant drugs of abuse²⁸, we found that mice voluntarily self-administered nicotine at all doses when tested in an oral nicotine intake paradigm (Fig. 1B, C), with a strong effect of dose across all experiments indicative of a titration effect^{29,30}. Mice showed the greatest preference for the nicotine solution at the 10 µg/ml concentration, where it represented 65–80% of their liquid intake. Adult mice exposed to NIC in adolescence consumed more nicotine solution as a percentage of their total liquid intake than their congeners exposed only to SAC in adolescence at all doses tested, (Fig. 1B *middle*, Table 1B), with differences in the daily

dose of nicotine most obvious at the 50 µg/ml and 100 µg/ml doses. This did not result from side bias in consumption, as all mice were able to track the position of the nicotine or sucrose solution (Supplementary Fig. 1G). In stark contrast, mice exposed to NIC in adulthood did not show different consumption behavior from their SAC-treated counterparts (Fig. 1C, Table 1E), suggesting that this 1-week pretreatment regimen is too mild to produce enduring changes to the adult brain. Liquid intake across the nicotine sessions was stable across all groups of mice, and only the mice pretreated with NIC in adolescence showed a significant difference from their SAC-treated counterparts in the volume (mL) of nicotine solution consumed (Supplementary Fig. 1D).

Nicotine has both reinforcing and anxiogenic properties²³, both of which have been hypothesized to contribute to addiction liability. We thus next investigated how exposure to NIC in adolescence affects the anxiogenic properties of acute nicotine delivery in the elevated O-Maze (EOM, Fig. 1D), or the reinforcing effects of nicotine in a conditioned place preference paradigm (CPP, Fig. 1D). We have previously found that naïve adult male mice show a pronounced, time-dependent reduction of time spent in the open arms of the EOM following nicotine administration²³. Here, we found that mice exposed to SAC in adolescence resembled our results in naïve mice: these mice showed an anxiogenic response to nicotine, as evidenced by a significant reduction in time spent in the open arms in the 6-to-9-minute block when compared to saline-injected counterparts. There was, however, no difference in time spent in the open arms in the 6-to-9-min block between saline and nicotine injected mice that were previously exposed to nicotine in adolescence, indicating that exposure to NIC in adolescence abolished this anxiogenic effect (Fig. 1E, Table 1G). However, the anxiogenic effect of acute nicotine injection was preserved in mice exposed to SAC or to NIC pretreatment as adults (Fig. 1H, Table 1I). Adult mice exposed to NIC in adolescence, but not those exposed in adulthood, were also impervious to reductions in open arm entries (Sup Fig. 1I) and suppression of locomotor activity (Supplementary Fig. 1I) in response to acute nicotine injection.

We have previously shown that adult male mice show CPP to a 0.5 mg/kg dose of nicotine³¹, but not to a 0.2 mg/kg dose of nicotine³². Here, we tested whether adult mice treated with nicotine in adolescence were more sensitive to the reinforcing effects of a low dose of nicotine. Mice exposed to SAC in adolescence did not show CPP to a 0.2 mg/kg dose of nicotine, in accordance with our previous results in naïve adult mice. However, mice treated with NIC in adolescence showed a significant preference for the nicotine-paired chamber at this same dose (Fig. 1F, Table 1H), suggesting that these mice are more sensitive to the reinforcing effects of nicotine. Mice treated with NIC or with SAC as adults showed no preference for the nicotine-paired chamber (Fig. 1I, Table 1J).

Together, these results define an adolescent period where exposure to nicotine produces an enduring profile of altered response to later nicotine, featuring a reduction of its anxiogenic properties, an increased sensitivity to its reinforcing properties, and an increase in voluntary consumption consistent with a vulnerable phenotype. This finding further suggests vulnerability to nicotine is titrated along an age spectrum, where ongoing developmental processes create resilience to the drug as adolescents progress into adulthood.

Nicotine in adolescence restructures nicotine-responsive networks in the adult brain

To dissect how this nicotine treatment in adolescence alters the functional organization of brain networks, we performed whole-brain activity mapping in a subset of mice that underwent testing in the EOM (Fig. 2A). Mice treated with NIC or SAC in adolescence or adulthood received an acute injection of nicotine or saline, were tested for anxiety-like behavior in the EOM, and were perfused -1 h later at peak cFos expression. Their brains were then cleared using iDISCO,

Table 1 | Detailed Statistics for Fig. 1

N	Test	Factor	Statistic	Statistic Value	p value	Corresponding Figure
A - % sucrose preference - adolescent pretreatment						
SAC = 21, NIC = 24	Shapiro-Wilk normality test		W	0.9478	0.0001	Fig. 1B left
	Wilcoxon rank sum test with continuity correction	SAC vs NIC at 0%	W	261.0000	1.0000*	
	Wilcoxon rank sum test with continuity correction	SAC vs NIC at 0.5%	W	256.0000	1.0000*	
	Wilcoxon rank sum test with continuity correction	SAC vs NIC at 1%	W	297.0000	0.9340*	
B - % nicotine preference - adolescent pretreatment						
SAC = 21, NIC = 24	Shapiro-Wilk normality test		W	0.9925	0.3077	Fig. 1B center
	Two-way mixed ANOVA	Interaction	F	1.1080	0.3544	
		Treatment (between subj)	F	8.4491	0.0058	
		Nic conc (within subjects)	F	68.2984	0.0000	
C - nicotine intake (mg/kg/day) - adolescent pretreatment						
SAC = 21, NIC = 24	Shapiro-Wilk normality test		W	0.8565	0.0000	Fig. 1B right
	Wilcoxon rank sum test with continuity correction	SAC vs NIC at 10 µg/mL	W	289.0000	0.4063*	
	Wilcoxon rank sum test with continuity correction	SAC vs NIC at 50 µg/mL	W	350.0000	0.0796*	
	Wilcoxon rank sum test with continuity correction	SAC vs NIC at 100 µg/mL	W	384.0000	0.0111*	
	Wilcoxon rank sum test with continuity correction	SAC vs NIC at 100 µg/mL	W	334.0000	0.1274*	
D - % sucrose preference - adult pretreatment						
SAC = 12, NIC = 12	Shapiro-Wilk normality test		W	0.8997	0.0000	Fig. 1C left
	Wilcoxon rank sum test with continuity correction	SAC vs NIC at 0%	W	73.0000	1.0000*	
	Wilcoxon rank sum test with continuity correction	SAC vs NIC at 0.5%	W	61.0000	1.0000*	
	Wilcoxon rank sum test with continuity correction	SAC vs NIC at 1%	W	69.0000	1.0000*	
E - % nicotine preference - adult pretreatment						
SAC = 12, NIC = 12	Shapiro-Wilk normality test		W	0.9803	0.0755	Fig. 1C center
	Two-way mixed ANOVA	Interaction	F	1.0332	0.3947	
		Treatment (between subj)	F	0.5357	0.4720	
		Nic conc (within subjects)	F	57.9616	0.0000	
F - nicotine intake (mg/kg/day) - adult pretreatment						
SAC = 12, NIC = 12	Shapiro-Wilk normality test		W	0.8945	0.0000	Fig. 1C right
	Wilcoxon rank sum test with continuity correction	SAC vs NIC at 10 µg/mL	W	46.0000	0.4229*	
	Wilcoxon rank sum test with continuity correction	SAC vs NIC at 50 µg/mL	W	31.0000	0.0775*	
	Wilcoxon rank sum test with continuity correction	SAC vs NIC at 100 µg/mL	W	56.0000	0.7417*	
	Wilcoxon rank sum test with continuity correction	SAC vs NIC at 100 µg/mL	W	71.0000	0.9770*	
G - % time in open arms of EOM - adolescent pretreatment						
SAC + SAL = 12, SAC + NIC = 16, NIC + SAL = 11, NIC + NIC = 14	Shapiro-Wilk normality test		W	0.8339	0.0000	Fig. 1E
	Kruskal-Wallis rank sum test	All groups, 0–3 min	Kruskal-Wallis chi-squared	0.8896	0.8279	
	Kruskal-Wallis rank sum test	All groups, 3–6 min	Kruskal-Wallis chi-squared	6.1815	0.1031	
	Kruskal-Wallis rank sum test	All groups, 6–9 min	Kruskal-Wallis chi-squared	14.4753	0.0023	
	Wilcoxon rank sum test with continuity correction	NIC-SAL vs NIC-NIC, 6–9 min	W	46.0000	0.2847*	
	Wilcoxon rank sum test with continuity correction	SAC-SAL vs SAC-NIC, 6–9 min	W	27.0000	0.0058*	
	Wilcoxon rank sum test with continuity correction	SAC-SAL vs NIC-SAL, 6–9 min	W	62.0000	0.8294*	

Table 1 (continued) | Detailed Statistics for Fig. 1

N	Test	Factor	Statistic	Statistic Value	p value	Corresponding Figure
H - CPP to 0.2 mg/kg nicotine - adolescent pretreatment	Wilcoxon rank sum test with continuity correction	SAC-NIC vs NIC-NIC, 6-9 min	W	146.5000	0.3117*	
	Shapiro-Wilk normality test		W	0.9628	0.3264	Fig. 1F
	One Sample t test	SAC difference from 0	t	-0.6684	0.5140	
	One Sample t test	NIC difference from 0	t	2.8120	0.0131	
I - % time in open arms of EOM - adult pretreatment	Welch Two Sample t-test	SAC vs NIC	t	2.3183	0.0277	
	Shapiro-Wilk normality test		W	0.7442	0.0000	Fig. 1H
	Kruskal-Wallis rank sum test	All groups, 0-3 min	Kruskal-Wallis chi-squared	1.0547	0.7880	
	Kruskal-Wallis rank sum test	All groups, 3-6 min	Kruskal-Wallis chi-squared	4.5444	0.2084	
J - CPP to 0.2 mg/kg nicotine - adult pretreatment	Kruskal-Wallis rank sum test	All groups, 6-9 min	Kruskal-Wallis chi-squared	18.3625	0.0004	
	Wilcoxon rank sum test with continuity correction	NIC-SAL vs NIC-NIC, 6-9 min	W	91.0000	0.0284*	
	Wilcoxon rank sum test with continuity correction	SAC-SAL vs SAC-NIC, 6-9 min	W	87.5000	0.0056*	
	Wilcoxon rank sum test with continuity correction	SAC-SAL vs NIC-SAL, 6-9 min	W	178.0000	1.0000*	
	Wilcoxon rank sum test with continuity correction	SAC-NIC vs NIC-NIC, 6-9 min	W	223.5000	1.0000*	
	Shapiro-Wilk normality test		W	0.9361	0.1337	Fig. 1I
	One Sample t test	SAC difference from 0	t	0.8596	0.4084	
	One Sample t test	NIC difference from 0	t	0.7025	0.4969	
	Welch Two Sample t-test	SAC vs NIC	t	0.0065	0.9949	

*Holm correction for multiple comparisons.

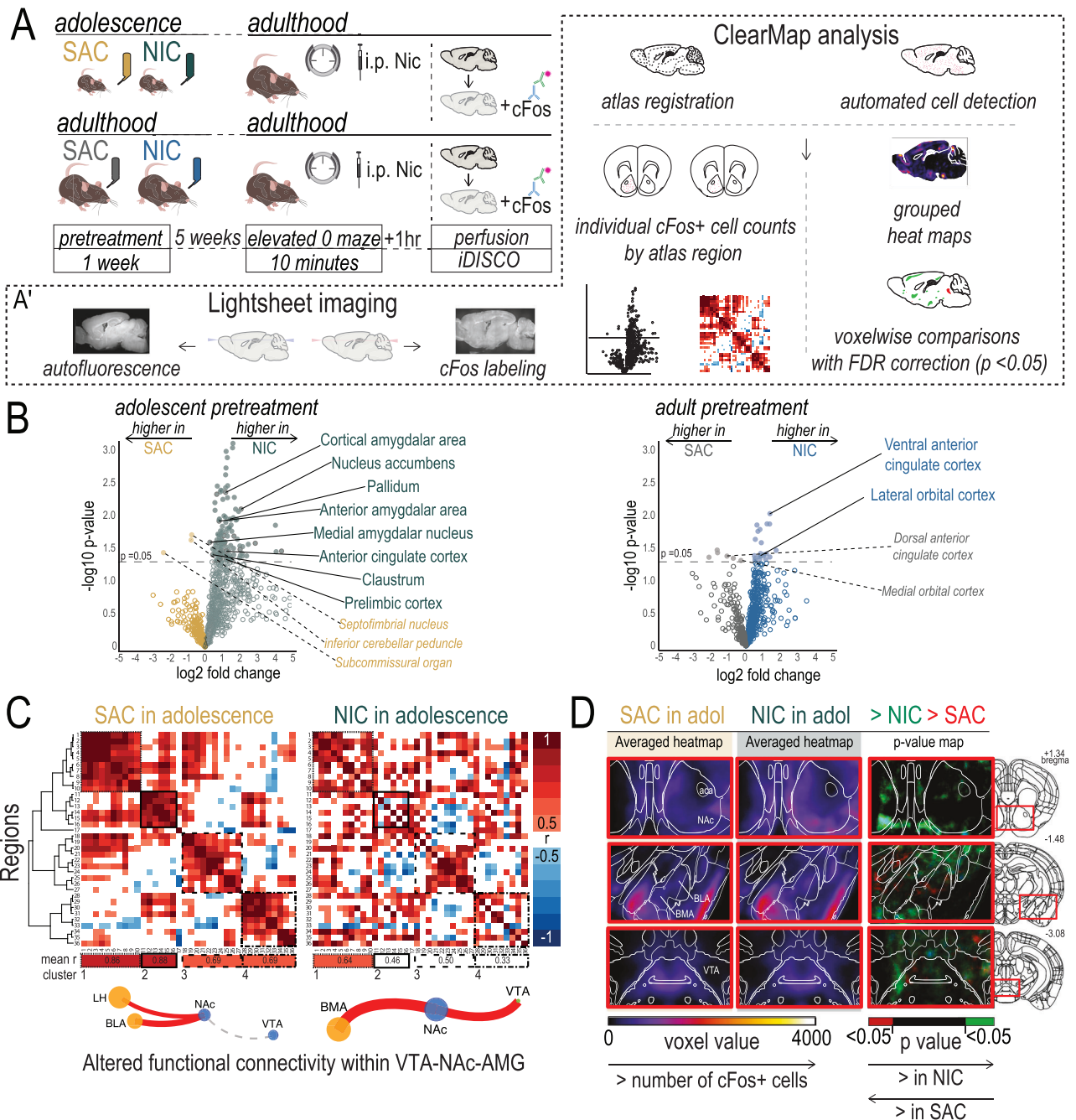


Fig. 2 | Nicotine in adolescence, but not in adulthood, reshapes brain-wide responsiveness to acute nicotine. **A** Experimental timeline for mice treated with Nicotine (NIC; 100 μ g/mL nicotine in 2% saccharin) or Saccharin (SAC; 2% saccharin only) in early adolescence or in adulthood. **A'** iDISCO brain clearing and Clearmap activity mapping pipeline. **B (Left)** Mice treated with NIC in adolescence show greater cFos activity across the brain, and in specific brain regions, following an acute nicotine injection when compared to their SAC-treated counterparts. Overall, 129 regions showed an increase in cFos activity in NIC-pretreated mice, defined as a fold change >0 and a $\log p > 1.3$ (equivalent to $p < 0.05$). Notable regions of interest associated with anxiety response and/or response to nicotine have been highlighted. **(Right)** The activation profile of mice treated with NIC in adulthood is not substantially different from their SAC-treated counterparts. Cell counts were compared with independent two-sample Student's t tests assuming unequal

variances, and p -values were converted to q -values to control for false discovery rate. **C** Correlation matrices of relationships between cFos cell numbers in response to nicotine injection. Activation across brain regions in SAC-pretreated mice (*left*) is highly correlated, and hierarchical clustering organizes these regions into 4 distinct modules with the strongest inter-region relationships. In NIC-pretreated mice (*right*), correlations between regions are less strong. **Bottom**, community analysis on networks formed from these correlation matrices indicate significant reorganization of the VTA-NAC-AMG connections. **D** Voxel-by-voxel analysis of these regions reveals increases in nicotine reactivity within the VTA and DA terminal regions. P-Value maps of significant differences between groups were generated from comparisons by independent two-sample Student's t tests assuming unequal variances. Green or red voxels indicate a $p < 0.05$ after FDR correction. All statistical comparisons were two-sided. Source data are provided as a Source Data file.

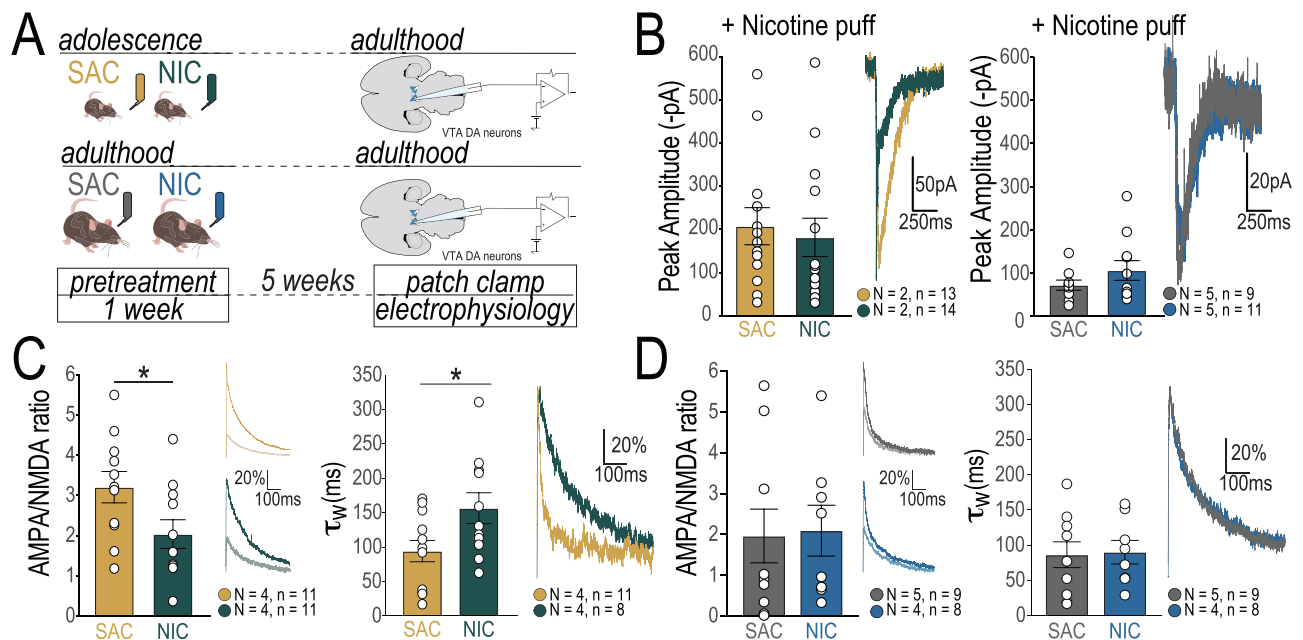


Fig. 3 | Persistent immature neurophysiological signature of VTA dopamine neurons in mice exposed to NIC in adolescence. **A** Experimental design for patch clamp experiments. **B Left:** No difference in peak amplitude of nicotine current between adult mice that received NIC or SAC as adolescents (NIC $N = 2$ mice, $n = 14$ neurons; SAC $N = 2$ mice, $n = 13$ neurons, Table 2A). **Right:** No difference in peak amplitude of nicotine current between adult mice that received NIC or SAC as adults (NIC $N = 5$ mice, $n = 11$ neurons; SAC $N = 5$ mice, $n = 9$ neurons, Table 2B). **C Left:** AMPA/NMDA ratio was decreased in mice that received NIC as adolescents (NIC $N = 4$ mice, $n = 11$ neurons; SAC $N = 4$ mice, $n = 11$ neurons, Table 2C). **Right:** NMDA current decay (weighted τ) was increased in mice that received NIC as

adolescents (NIC $N = 4$ mice, $n = 11$ neurons; SAC $N = 4$ mice, $n = 11$ neurons, Table 2D). **D Left:** No differences in AMPA/NMDA ratio were observed when mice received NIC as adults (NIC $N = 4$ mice, $n = 8$ neurons; SAC $N = 5$ mice, $n = 9$ neurons, Table 2E). **Right:** NMDA current decay (weighted τ) was the same between mice that received NIC or SAC as adults (NIC $N = 4$ mice, $n = 8$ neurons; SAC $N = 5$ mice, $n = 9$ neurons, Table 2F). All bar graphs are presented as mean values \pm SEM. * $p < 0.05$, ** $p < 0.01$, *** $p < 0.01$. All statistical comparisons were two-sided. Detailed information about statistical testing is available in Table 2. Source data are provided as a Source Data file.

received SAC or NIC as adults did not show differences in the voxel-by-voxel comparison of grouped cell counts across these same regions (Supplementary Fig. 2F). These results identify functional changes, particularly within dopaminergic networks, present in adult animals following exposure to NIC in adolescence, which may underlie the vulnerability to nicotine use we observed in these mice.

Immature dopamine neuron physiology persists in adult mice exposed to nicotine in adolescence

While we discovered significant perturbation in DAergic functional networks following adolescent exposure to NIC in our brain-wide activity analysis, including changes in activation in the NAc and AMG regions, we did not find changes in DA bouton density in these terminal regions (Supplementary Fig. 3A–D). Thus, we next assessed the electrophysiological profiles of DA neurons (Fig. 3A) to elucidate whether network changes may result from altered DA neuron responsiveness to nicotine. The peak amplitude of nicotine currents did not differ between mice exposed to NIC or SAC in adolescence (Fig. 3B left, Table 2A) or adulthood (Fig. 3B right, Table 2B), however NIC treated mice showed faster response kinetics and an associated reduction in charge transferred (Supplementary Fig. 3E), suggesting that signaling through nAChR receptors may be altered in the VTA of these mice. Presynaptic release probability of excitatory synapses onto DA neurons did not appear to be altered in NIC exposed mice (Supplementary Fig. 3G), however we found striking differences in excitatory post-synaptic currents (Supplementary Fig. 3H) and plasticity on DA neurons only of adult mice exposed to NIC in adolescence. These mice showed a reduction in AMPA/NMDA ratio in comparison to SAC-treated controls (Fig. 3C left, Table 2C) and an increase in the weighted NMDA decay time constant (τ_w , Fig. 3C right, Table 2D), albeit without a clear contribution of changes to NR2B subunit expression

(Supplementary Fig. 3F). The changes were not present in mice exposed to nicotine as adults (Fig. 3D, Table 2E, F). Interestingly, these alterations to glutamatergic plasticity onto VTA dopamine neurons of adult mice exposed to NIC as adolescents resemble some conditions observed in young brains^{16,41–44}, suggesting that NIC exposure in adolescence may impede the maturation of glutamatergic plasticity mechanisms.

To determine if mice also maintain an adolescent-like response to nicotine injection after adolescent exposure, we first defined adult and adolescent responses to nicotine using in vivo single unit recordings in anesthetized mice (Fig. 4A). Dopamine neurons of naïve adult male mice show opposing responses to intravenous nicotine administration, with >90% of neurons projecting to the nucleus accumbens (NAc) activated in response to nicotine, and the >85% of neurons projecting to the amygdala (Amg) inhibited by nicotine in a previous study²³. We first replicated this same distribution in adult mice, with DA neurons (identified by their electrophysiological characteristics and confirmed with neurobiotin labeling in a subset of neurons) showing both excitatory (putative VTA-NAc circuit) and inhibitory (putative VTA-Amg circuit) responses to i.v. nicotine injection (Fig. 4B, bottom). Next, we discovered that this pattern is already apparent in early adolescence, with DA neurons both activated or inhibited by nicotine present in the VTA (Fig. 4B, top). Dopamine neurons from naïve adolescent mice, however, showed a higher maximum activation in response to nicotine injection when compared to naïve adults (Fig. 4C, Table 3A), while there was no difference in the level of DA neuron inhibition by nicotine between the ages (Table 3B). The fact that DA neuron responses to nicotine in adolescent animals are “imbalanced”, or are stronger in activation of the VTA-NAc pathway, may represent a physiological vulnerability signature, in line with reports of greater rewarding effects of nicotine in adolescent animals⁸.

Table 2 | Detailed Statistics for Fig. 3

N	Test	Factor	Statistic	Statistic Value	p value	Corresponding Figure
A - Nicotine current - adolescent pretreatment						
NIC = 2 mice, 14 neurons; SAC = 2 mice, 13 neurons	Shapiro-Wilk normality test		W	0.8553	0.0015	Fig. 3B
	Wilcoxon rank sum test with continuity correction	SAC vs NIC	W	108.0000	0.4233	
B - Nicotine current - adult pretreatment						
NIC = 5 mice, 11 neurons; SAC = 5 mice, 9 neurons	Shapiro-Wilk normality test		W	0.8200	0.0017	Fig. 3B
	Wilcoxon rank sum test with continuity correction	SAC vs NIC	W	42.0000	0.5949	
C - AMPA/NMDA Ratio - adolescent pretreatment						
NIC = 4 mice, 11 neurons; SAC = 4 mice, 11 neurons	Shapiro-Wilk normality test		W	0.9603	0.4963	Fig. 3C
	Welch Two Sample t-test	SAC vs NIC	t	-2.2008	0.0398	
D - Weighted Tau - adolescent pretreatment						
NIC = 4 mice, 8 neurons; SAC = 4 mice, 11 neurons	Shapiro-Wilk normality test		W	0.9474	0.2808	Fig. 3C
	Welch Two Sample t-test	SAC vs NIC	t	2.2914	0.0343	
E - AMPA/NMDA Ratio - adult pretreatment						
NIC = 4 mice, 8 neurons; SAC = 5 mice, 9 neurons	Shapiro-Wilk normality test		W	0.8319	0.0057	Fig. 3D
	Wilcoxon rank sum test with continuity correction	SAC vs NIC	W	39.5000	0.7727	
F - Weighted Tau - adult pretreatment						
NIC = 4 mice, 8 neurons; SAC = 5 mice, 9 neurons	Shapiro-Wilk normality test		W	0.9380	0.2949	Fig. 3D
	Welch Two Sample t test	SAC vs NIC	t	0.1470	0.8851	

We next assessed VTA dopamine neuron firing in adult mice exposed to SAC or NIC during adolescence or during adulthood (Fig. 4D). We found that all groups of mice showed a spectrum of response to nicotine as observed in naïve animals, with responses again ranging from strong activation to strong inhibition by nicotine (Fig. 4E). Interestingly, mice exposed to nicotine in adolescence showed a stronger, adolescent-like, activation of DA neurons in response to nicotine than their SAC treated counterparts, with no change in the magnitude of inhibition (Fig. 4F, Table 3C, D). This result suggests that there is greater activation in the VTA-NAc pathway in the NIC pre-treated mice. This effect was not observed in mice exposed to nicotine as adults (Fig. 4G, Table 3E, F), suggesting that nicotine in adolescence promotes the persistence of an endogenous adolescent state when the effects of nicotine are skewed in favor of its rewarding effect.

Restoring adult-like balance in nicotine-evoked DA signaling unmask mature behavioral response

Our electrophysiological results raise the intriguing hypothesis that exposure to nicotine in adolescence “freezes” dopamine circuitry in an imbalanced, immature state, which promotes vulnerability to nicotine use. More concretely, this means that exposure to nicotine in adolescence prevented the maturation of the dopamine system, keeping its response to nicotine in a persistent adolescent-like state. We next sought to test whether adolescent-like DA functioning would explain the differences that we observed in the behavioral response to nicotine following preexposure in adolescence. We thus tested naïve adult and adolescent mice for CPP to a 0.2 mg/kg dose of nicotine and for nicotine-induced anxiety-like behavior in the EOM to establish whether there is a basal difference between adolescents and adults in these nicotine responses. Naïve adolescent or adult mice underwent a 5-day CPP paradigm where either one compartment was paired with saline and one with 0.2 mg/kg of nicotine, or both chambers were paired with saline. Multiple previous studies have shown that adolescent rodents show CPP to lower doses of nicotine than adult rodents do⁴⁵⁻⁴⁷. We

indeed found that adolescent mice showed a robust place preference to nicotine (Fig. 5A center, Table 4A), while adult mice showed no preference for the nicotine-paired chamber (Fig. 5A right, Table 4B), in line with our previous findings³².

In accordance with our previous results²³, naïve adult mice showed a decrease in time spent in the open arms of the EOM following an i.p. injection of nicotine, but not after an injection of saline, indicating an anxiety-like response to nicotine (Fig. 5B right, Table 4D). However, when mice were tested at PND 28 this anxiety-like response to nicotine was absent, as the mice showed no difference in time spent in the open arms after nicotine or saline injection (Fig. 5B center, Table 4C), in line with results from adolescent rats⁴⁸. As this strongly resembled the behavioral effect that we observed in mice treated with NIC in adolescence (Fig. 1E), this result suggests that not only does nicotine in adolescence block both neural and behavioral responses to nicotine in an immature state, but that imbalance between nicotine-induced activation and inhibition of VTA dopamine neurons could be actively masking the anxiogenic effect of the drug.

While increased place preference to nicotine in adolescent and adolescent-pretreated animals can be explained by the augmented nicotine response in NAc-projecting VTA dopamine neurons, as specifically stimulating this pathway promotes place preference²³, the mechanism underlying the abolishment of nicotine induced anxiety is unknown. If the exaggerated, adolescent-like VTA-NAc DA neuron response to nicotine in adult mice exposed to NIC as adolescents is masking the anxiogenic effects of the drug, dampening the activity of this circuit during nicotine administration could reveal the mature response. To test this possibility, we used a chemogenetic approach to exclusively decrease the excitability of VTA DA neurons of mice exposed to NIC in adolescence⁴⁹, by expressing an inhibitory DREADD (hM4D(G_i)) in a projection- and neurotransmitter-specific manner (Fig. 5C). Mice that received the control virus recapitulated our previous results (Fig. 1E) of an abolished anxiogenic response to nicotine in adults previously exposed to NIC in adolescence (Fig. 5D center). In contrast, dampening VTA-NAc DA activity with the DREADD virus

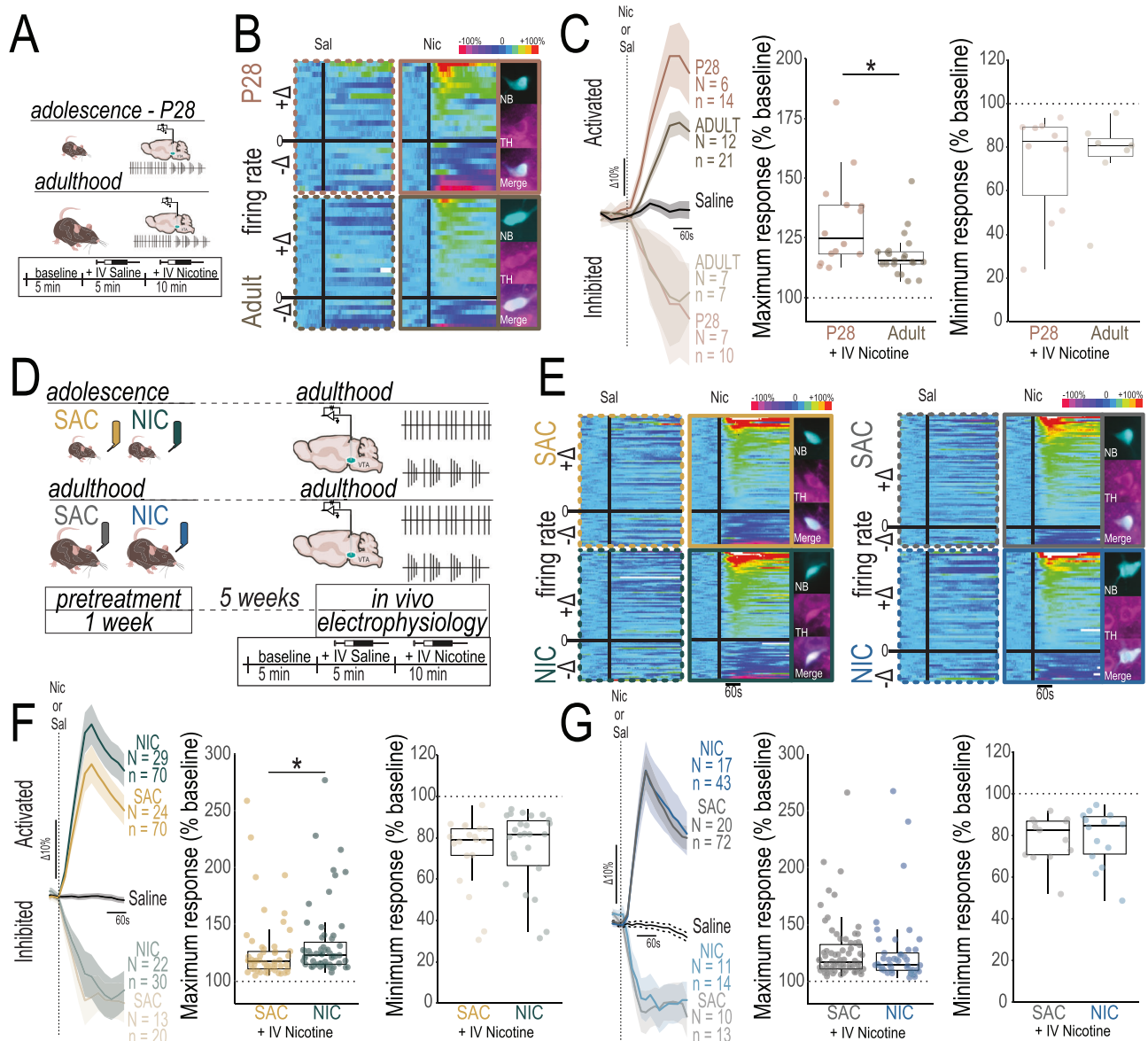


Fig. 4 | An adolescent-like imbalance in VTA dopamine neuron response to nicotine persists in adult mice exposed to nicotine in adolescence.

A Experimental design. **B** Neuron responses to saline (Sal) or nicotine (Nic) injection represented as changes from baseline activity in adolescent (P28) mice (*Top*) and adult (>P60) mice (*Bottom*). *Insets*: Example neurons were labeled with neurobiotin (NB) and tyrosine hydroxylase (TH) to confirm their dopaminergic identity. **C** Nicotine evoked activation was increased in dopamine neurons of adolescent mice in comparison with adults (*center*, Adolescent $N=6$ mice, $n=14$ neurons; Adult $N=12$ mice, $n=21$ neurons, Table 3A), with no difference in inhibition (*right*, Adolescent $N=7$ mice, $n=7$ neurons; Adult $N=7$ mice, $n=10$ neurons, Table 3B). **D** Experimental design. **E** Neuron responses to Sal or Nic injection in adolescent-treated mice (*left*) and adult-treated mice (*right*). *Insets*: NB + TH+ example neurons. **F** Nicotine evoked activation was increased in dopamine neurons of adult

mice treated with NIC in adolescence in comparison with SAC-treated counterparts (*center*, NIC $N=29$ mice, $n=70$ neurons; SAC $N=24$ mice, $n=70$ neurons, Table 3C), with no difference in inhibition (*right*, NIC $N=22$ mice, $n=30$ neurons; SAC $N=13$ mice, $n=20$ neurons, Table 3D). **G** Nicotine evoked activation did not differ between dopamine neurons of mice treated with NIC or SAC as adults (*center*, NIC $N=17$ mice, $n=43$ neurons; SAC $N=20$ mice, $n=72$ neurons, Table 3E) nor in inhibition (*right*, NIC $N=11$ mice, $n=14$ neurons; SAC $N=10$ mice, $n=13$ neurons, Table 3F). Line graphs are presented with lines as mean values and shaded regions as \pm SEM. Box plots include a box extending from the 25th to 75th percentiles, with the median indicated by a line and with whiskers extending from the minima to the maxima. * $p < 0.05$, ** $p < 0.01$, *** $p < 0.01$. All statistical comparisons were two-sided. Detailed information about statistical testing is available in Table 3. Source data are provided as a Source Data file.

caused the mice to spend dramatically less time in the open arms of the EOM after i.p. nicotine injection (Fig. 5D *right*, Table 4E), an effect closely resembling the response to nicotine in naïve adults (Fig. 5B *right*) and in adult mice treated with SAC in adolescence (Fig. 1E). However, both mCherry and DREADD injected mice that received CNO one hour before being tested with saline in the EOM showed similar levels of exploration of the open arms, in line with our other experiments, indicating that (1) exposure to the CNO *itself* does not produce an anxiogenic or anxiolytic effect, and (2) decreasing the excitability of

the VTA-Nac pathway alone (i.e., the hM4D(Gi)-SAL condition) does not produce an anxiogenic or anxiolytic effect. The DREADD + nicotine mice were the only group tested that showed a significant anxiogenic response in the EOM, indicating that decreasing the excitability of VTA-Nac DA neurons restored the mature behavioral response to nicotine, effectively unmasking the anxiogenic effect of the drug. Together, our results suggest that NIC in adolescence perpetuates a developmental signaling imbalance between discrete DA circuits in response to nicotine which masks the anxiogenic effect of the drug, leading to a

Table 3 | Detailed Statistics for Fig. 4

N	Test	Factor	Statistic	Statistic Value	p value	Corresponding Figure
A - maximum activation - naïve animals						
Adolescent = 14, Adult = 21	Shapiro-Wilk normality test		W	0.7851	0.0000	Fig. 4C
	Wilcoxon rank sum test with continuity correction	Adolescent vs. Adult	W	215.0000	0.0230	
B - maximum inhibition - naïve animals						
Adolescent = 10, Adult = 7	Shapiro-Wilk normality test		W	0.8089	0.0027	Fig. 4C
	Wilcoxon rank sum test with continuity correction	Adolescent vs. Adult	W	37.0000	0.8836	
C - maximum activation - adolescent pretreatment						
NIC = 70, SAC = 68	Shapiro-Wilk normality test		W	0.6534	0.0000	Fig. 4F
	Wilcoxon rank sum test with continuity correction	NIC vs SAC	W	1748.0000	0.0072	
D - maximum inhibition - adolescent pretreatment						
NIC = 30, SAC = 21	Shapiro-Wilk normality test		W	0.7946	0.0000	Fig. 4F
	Wilcoxon rank sum test with continuity correction	NIC vs SAC	W	262.0000	0.3150	
E - maximum activation - adult pretreatment						
NIC = 45, SAC = 72	Shapiro-Wilk normality test		W	0.6465	0.0000	Fig. 4G
	Wilcoxon rank sum test with continuity correction	NIC vs SAC	W	1810.0000	0.2884	
F - maximum inhibition - adult pretreatment						
NIC = 14, SAC = 13	Shapiro-Wilk normality test		W	0.9032	0.0158	Fig. 4G
	Wilcoxon rank sum test with continuity correction	NIC vs SAC	W	84.0000	0.7524	

vulnerability to increased nicotine taking in adult animals. Furthermore, our findings from the DREADD experiments indicate that this imbalance can be rescued by targeted pathway manipulations.

Discussion

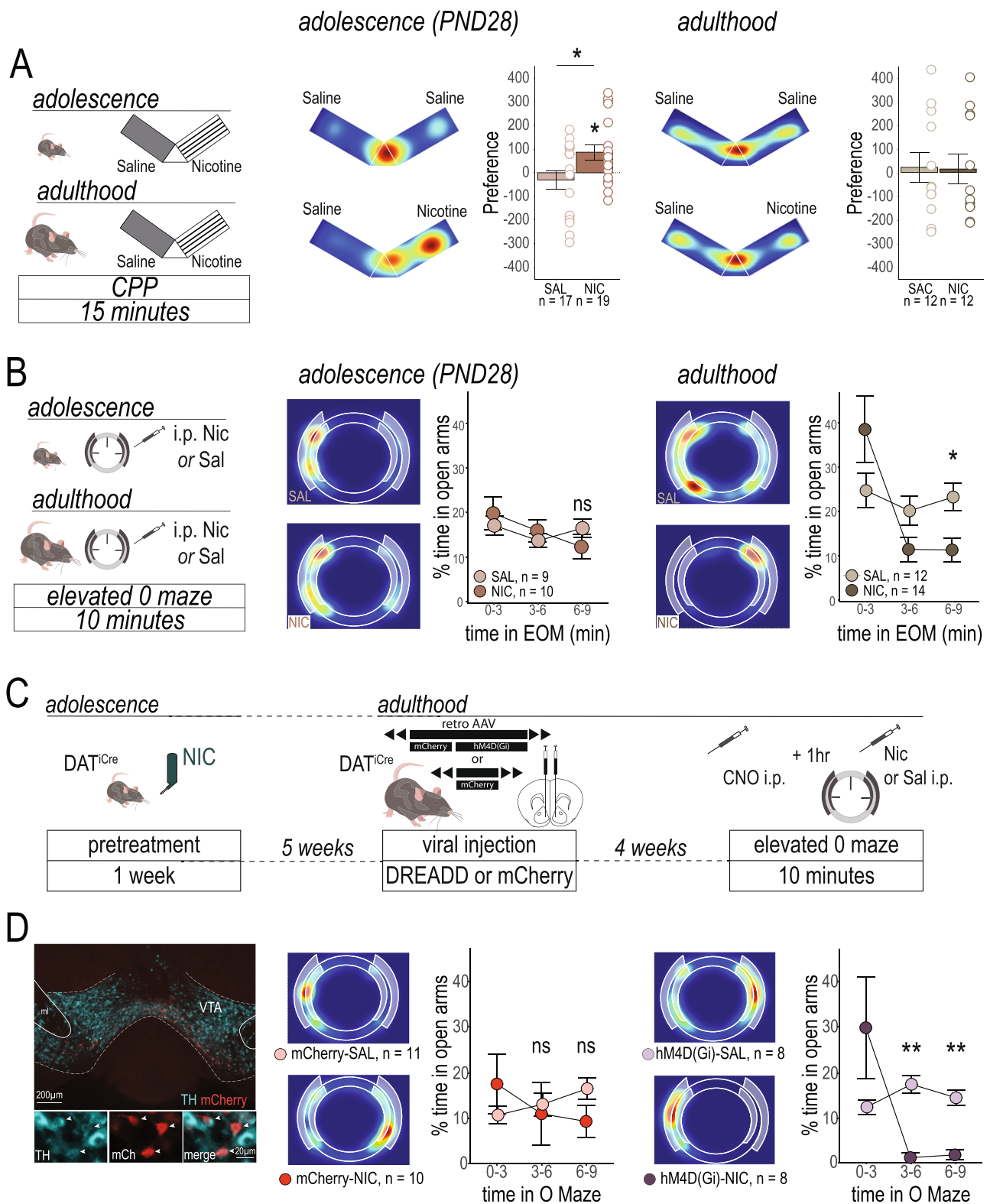
Nicotine use in adolescence remains a serious public health issue, with strong associations between early onset of use and later addiction⁴. Moreover, the widespread availability and acceptability of e-cigarette use has facilitated a startling increase in number of adolescent users and a concomitant decrease in their age of onset^{26,50}. Understanding how nicotine in adolescence impacts developing neural circuits is essential for informing evidence-based intervention efforts. We propose that exposure to nicotine in adolescence prolongs a developmental imbalance in dopaminergic circuitry and in behavioral response to nicotine re-exposure, which, in turn, can promote vulnerability to nicotine use and addiction.

Mesocorticolimbic DA circuits are known to undergo extraordinary growth and remodeling in the adolescent brain¹¹, in contrast to other neuromodulatory systems which are largely established at the start of adolescence. As such, the DA system is known to be sensitive to experience in adolescence, with significant effects of stress, social isolation, and drug use persisting until adulthood in many cases^{10,11}. While VTA DA neurons are often considered as a single population, DA neurons in fact show significant physiological and molecular heterogeneity, which are associated with differences in their input-output wiring^{43,51}. Increasingly, these diverse DA pathways are shown to play divergent roles in behavior, including responses to drugs of abuse^{20,23,52,53}. With regards to nicotine response, we have shown that VTA-NAc projecting neurons are activated by nicotine, while VTA-AMg projecting neurons are inhibited by nicotine in adult mice, leading, respectively, to the expression of the reinforcing and anxiogenic properties of behavioral response to the drug²³. How exactly adolescent experiences shape dopaminergic function within these distinct circuits is still an open question, with possibilities including to advance, slow, or misroute normal maturational processes. Here, our evidence suggests that experience with nicotine in adolescence arrests the development of VTA-NAc and VTA-AMg DA circuits, keeping them in a prolonged adolescent state. This stalling of developing DA circuits in response to experience is likely not limited to nicotine, or even drug exposure, as similar changes in glutamate plasticity onto VTA DA

neurons have been reported after food insecurity in adolescence⁵⁴. This raises important questions in the cross-sensitivity and additive relationship between stress and drug use in adolescence and adulthood. Other studies have reported pathological miswiring of DA circuits after psychostimulant exposure in adolescence^{10,25}. While our evidence does not support the idea that nicotine in early adolescence leads to the global miswiring of dopamine axons, as the innervation patterns of dopamine axons in the NAc and AMG are unchanged, we find, rather, the persistent maintenance of adolescent-like responses to an acute nicotine challenge. Importantly, we also provide evidence that adult-like behavior can be restored by artificially re-calibrating neural responses to adult levels.

Our 1-week nicotine exposure paradigm is not sufficient to cause behavioral or physiological changes when this exposure occurs during adulthood. However, when this same exposure regimen is administered during adolescence, it produces enduring alterations to the response to a later nicotine challenge, priming the VTA-NAc dopamine pathway, specifically, to be more reactive to nicotine. This is in line with work showing that the acute and enduring effects of nicotine on the adolescent brain differ from those in adults. Notably, adolescent rodents are thought to be more sensitive to the rewarding effects of nicotine, as well as less sensitive to its aversive effects, than adult animals^{8,48}. The naturally occurring development of brain circuitry between adolescence and adulthood can thus be viewed as a protective mechanism against the deleterious effects of experience, and of nicotine use in particular. We found that the behavioral and physiological response to acute nicotine in adult mice pretreated with nicotine in adolescence strongly resembles the response of naïve adolescent mice. This finding suggests that nicotine exposure in adolescence blocks the protective normative maturation of nicotine-responsive systems and results in discordance between rewarding and aversive nicotine signals. We propose that this may be one mechanism by which nicotine use in adolescence creates an enduring vulnerability to later nicotine use and addiction. An imbalance between the rewarding and aversive effects of nicotine has indeed been posited as a mechanism driving the transition from casual use to addiction^{29,55–57}.

We focused our nicotine treatment on the early adolescent period (-PND21-28) because not only does this correspond to the time of life when human adolescents are most likely to begin nicotine use^{26,27}, but previous work in rodent models has also suggested that this is a



particularly vulnerable time for DA development^{25,58}. Importantly, marked sex differences exist in adolescent developmental trajectories, including dopamine development¹¹. Recent work has shown that adolescent periods of DA circuit vulnerability to experience differ between male and female mice, and that even when the immediate effects of an experience are the same, the enduring outcomes may differ dramatically due to sex- and/or age specific compensatory processes²⁵. Nicotine receptor expression and function can be modulated by female sex

hormones⁵⁹, suggesting that even the immediate experience or effects of nicotine may be sex-dependent, adding to the complexity of addressing sex and developmental interactions in its effects. Ongoing work will address whether female mice show a similar or different pattern of adolescent DA circuit “freezing” by nicotine. Differential ages of vulnerability between sexes are also a key research arena, taking into account data from human studies showing that boys begin using nicotine younger than girls do⁶⁰, and are more likely to

Fig. 5 | Chemogenetically dampening VTA-NAC circuit activity restores anxiety-like response to nicotine in adult mice exposed to nicotine in adolescence.

A Experimental timeline for naïve mice (*left*). Following a 5-day CPP paradigm, adolescent mice showed a significant place preference for the chamber paired with 0.2 mg/kg nicotine (*center*, Table 4A), while adult mice did not (*right*, Table 4B). **B** Experimental timeline for naïve mice (*left*). Adolescent mice show no difference in the time spent in the open arms of the EOM between a saline or nicotine injection (*center*, Table 4C). Adult mice spend less time in the open arms of the EOM following an injection of nicotine than an injection of saline (*right*, Table 4D), indicative of an anxiogenic effect of nicotine. **C** Experimental timeline for DREADD intervention experiment. DAT^{Cre} mice were pretreated with NIC in adolescence, and then as adults they received an injection of a retroAAV hM4D(Gi) or control fluorescent-reporter virus into the NAC at the level of the medial shell. After 4 weeks, mice received an injection of CNO one hour before an injection of nicotine

or saline and entering the EOM. **D** Retro AAV viruses were well expressed in VTA DA neurons of DAT^{Cre} mice following their behavioral testing (*left*). Mice that received a control virus replicated the effect of NIC in adolescence on WT mice, as mice never spent less time in the open arms of the EOM than their saline-treated counterparts (*center*, Table 4E). When VTA-NAC DA activity was reduced before nicotine injection, however, a mature behavioral response to nicotine injection, where mice spend less time in the open arms of the EOM, was restored (*right*, Table 4E). All line graphs are presented as mean values \pm SEM. Graphs are separated by pre-treatment group for clarity, but statistical analyses compared all four treatment conditions. Heatmaps are from representative individual animals. * $p < 0.05$, ** $p < 0.01$, *** $p < 0.001$, ns = not significant. All statistical comparisons were two-sided. Holm's sequential Bonferroni corrections were used to correct for multiple comparisons. Detailed information about statistical testing is available in Table 4. Source data are provided as a Source Data file.

escalate nicotine intake by transitioning from e-cigarette to cigarette use⁶¹.

Why adolescent nicotine users are more likely to continue to use nicotine, to have longer and heavier smoking careers, and to develop cross-drug addictions and/or psychiatric symptoms has largely remained unexplained at a mechanistic level. The oral nicotine consumption paradigm used in the current studies cannot be considered a direct model of adolescent nicotine use in humans, notably as the route of nicotine administration (and thus its pharmacokinetic properties⁶²), the dosing, and the metabolism of the drug differ between species. However, here we are able to show that exposure to nicotine during a discrete period in adolescence locks the function of DA neurons in a persistent adolescent-like state, leading to exaggerated response to the rewarding effects of nicotine and a blunting of its negative, anxiogenic effects. This adolescent-like bias in behavioral responding may therefore facilitate the transition from casual use to addiction across the lifetime. Because we were able to restore an adult-like behavioral response to nicotine with a chemogenic approach, our findings suggest that these effects of nicotine in adolescence may be reversible. Developing interventions that target restoring an appropriate balance between the positive and negative effects of nicotine use may have therapeutic applications.

Methods

Animals

All experiments and procedures were performed in accordance with European Commission directives 219/1990, 220/1990 and 2010/63, and approved by Sorbonne Université and the ethical committee (CEEA) #005 under the protocol number 00553.02, or by the ESPCI and the ethical committee #059 under APAFIS#24037-2020102011276492. Wild-type (WT) C57BL/6 mice (Janvier Labs, France) or DAT^{Cre} mice (from François Tronche⁶³) were maintained on a 12-h light–dark cycle (light on at 0800 h), at an average temperature of 21 degrees and ~50% humidity. Mice were given ad libitum access to food and water unless noted.

Drugs

Pretreatment regimen. Nicotine tartrate salt (Glentham Biosciences) was dissolved into a 2% Saccharin (Sigma) solution to a final concentration of 100 μ g/mL and pH was adjusted to 7.2 ± 0.2 . Mice had access to either the nicotine solution or a 2% saccharin solution during one week.

Experimental solutions. Nicotine tartrate salt was solubilized in a physiological saline solution (0.9% NaCl) with pH adjusted to 7.2 ± 0.2 , and was injected intravenously (IV) at a 30 μ g/kg dose for juxtacellular recordings, or intra-peritoneally (IP) at a 0.5 mg/kg dose for the elevated O-maze (EOM) test and for the activity mapping experiment. For the Two bottle choice task, Nicotine tartrate salt was dissolved in water to a final concentration of 10 μ g/mL, 50 μ g/mL, 100 μ g/mL, or

200 μ g/mL and pH was adjusted to 7.2 ± 0.2 . All concentrations are expressed as free base.

Behavior

Two-bottle choice. Mice were single-housed in a cage with two drinking bottles where the volume change was measured continuously every minute with an automated acquisition system (TSE system, Germany). Mice were first presented with water in both bottles for a four-day habituation period, and the position of the bottles (i.e., right or left side of the cage) was swapped after 2 days. For each of the test solutions the same pattern was used; mice had access to each of the solutions tested during 4 consecutive days, and the position of the test solution was changed every 2 days (Fig. 1A). Mice were first tested for sucrose preference by changing the solution in one bottle to a 0.5% sucrose solution, while the other continued to contain plain water. After 4 days, the test solution was changed to 1% sucrose. Nicotine preference was tested with consecutively increasing doses of nicotine (10, 50, 100 and 200 μ g/ml, free base) in the test bottle, the control bottle remained full of plain water. Sweetening the nicotine and control solution with saccharin was avoided as it can obscure the difference in value between the two choices^{64–67}. Mice were weighed every other day to quantify the nicotine intake in mg/kg/day. Mice showing a strong side bias (preference <20% or >80% for one side) during the habituation period were removed from the analyses. While measurements took place continuously, sessions were defined as running overnight each test day from 20:00 to 14:00, encompassing the most active drinking periods of the day (Fig. 1B) and homogenizing the measurement periods between days with continuous recording and days when the recording had to be stopped in order to change the position and/or contents of the bottles. All solution changes thus occurred during the 14:00–20:00 ‘off’ time window. Minute-by-minute measurements were thresholded at a value of 0.1 ml, with values greater than 0.1 ml/min representing less than 0.01% of the full data set and considered to be erroneous measurements (leaking, sensor issue).

Elevated O-maze test. All behavioral tests were conducted during the light period of the animal cycle (between 1:00 and 7:00PM). The raw data for behavioral experiments were acquired as video files. The elevated O-maze (EOM) apparatus consists of two open (stressful) and two enclosed (protecting) elevated arms that together form a zero or circle (diameter of 50 cm, height of 58 cm, 10 cm-wide circular platform). Time spent in exploring enclosed versus open arms indicates then the anxiety level of the animal. The test lasts 10 min: mice are injected 1 min before the test, and then put in the EOM for 9 min. Mice are placed in an open arm at one of the four entrances of a closed arm, with the entrance (e.g., 1–4) distributed pseudorandomly across the experiment. Time spent in open or closed arms was extracted frame-by-frame using the open-source video analysis pipeline ezTrack⁶⁸. Mice were habituated to the stress of handling and injection for a minimum of one week before testing.

Table 4 | Detailed Statistics for Fig. 5

N	Test	Factor	Statistic	Statistic Value	p value	Corresponding Figure
A - CPP to 0.2 mg/kg nicotine - naïve adolescents						
SAL = 17, NIC = 19	Shapiro-Wilk normality test		W	0.9712	0.4605	Fig. 4A center
	One Sample t test	SAL difference from 0	t	-0.7875	0.4425	
	One Sample t test	NIC difference from 0	t	2.7048	0.0145	
	Welch Two Sample t test	SAC vs NIC	t	2.3317	0.0262	
B - CPP to 0.2 mg/kg nicotine - naïve adults						
SAC = 12, NIC = 12	Shapiro-Wilk normality test		W	0.8885	0.0124	Fig. 4A right
	One Sample t-test	SAC difference from 0	t	0.3367	0.7427	
	One Sample t-test	NIC difference from 0	t	0.2286	0.8234	
	Welch Two Sample t-test	SAC vs NIC	t	-0.0797	0.9372	
C - % time in open arms of EOM - naïve adolescent animals						
SAL = 9, NIC = 10,	Shapiro-Wilk normality test		W	0.9832	0.6108	Fig. 4B center
	Welch Two Sample t-test	NIC vs. SAC in 0–3 min	t	0.6447	0.9308*	
	Welch Two Sample t-test	NIC vs. SAC in 3–6 min	t	0.7492	0.9308*	
	Welch Two Sample t-test	NIC vs. SAC in 6–9 min	t	-1.2011	0.7408*	
D - % time in open arms of EOM - naïve adult animals						
SAL = 12, NIC = 14,	Shapiro-Wilk normality test		W	0.8876	0.0000	Fig. 4B right
	Wilcoxon rank sum test with continuity correction	NIC vs. SAC in 0–3 min	W	104.0000	0.3159†	
	Wilcoxon rank sum test with continuity correction	NIC vs. SAC in 3–6 min	W	51.0000	0.1891†	
	Wilcoxon rank sum test with continuity correction	NIC vs. SAC in 6–9 min	W	35.0000	0.0377†	
E - % time in open arms of EOM - DREADDS						
MCH + SAL = 11, MCH + NIC = 10,	Shapiro-Wilk normality test		W	0.7376	0.0000	Fig. 4C
HM4 + SAL = 11, HM4 + NIC = 14	Kruskal-Wallis rank sum test	All groups, 0–3 min	Kruskal-Wallis chi-squared	1.7264	0.6311	
	Kruskal-Wallis rank sum test	All groups, 3–6 min	Kruskal-Wallis chi-squared	18.0767	0.0004	
	Kruskal-Wallis rank sum test	All groups, 6–9 min	Kruskal-Wallis chi-squared	16.4805	0.0009	
	Wilcoxon rank sum test with continuity correction	HM4-SAL vs HM4-NIC, 3–6 min	W	1.0000	0.0033†	
	Wilcoxon rank sum test with continuity correction	MCH-SAL vs MCH-NIC, 3–6 min	W	29.0000	0.1846†	
	Wilcoxon rank sum test with continuity correction	MCH-SAL vs HM4-SAL, 3–6 min	W	56.0000	0.1846†	
	Wilcoxon rank sum test with continuity correction	MCH-NIC vs HM4-NIC, 3–6 min	W	21.0000	0.3423†	
	Wilcoxon rank sum test with continuity correction	HM4-SAL vs HM4-NIC, 6–9 min	W	1.0000	0.0040†	
	Wilcoxon rank sum test with continuity correction	MCH-SAL vs MCH-NIC, 6–9 min	W	28.0000	0.1368†	
	Wilcoxon rank sum test with continuity correction	MCH-SAL vs HM4-SAL, 6–9 min	W	37.0000	0.1368†	
	Wilcoxon rank sum test with continuity correction	MCH-NIC vs HM4-NIC, 6–9 min	W	18.0000	0.5915†	

†Holm correction for multiple comparisons.

Conditioned place preference (CPP). CPP experiments were performed in a Y-maze apparatus (Imetronic, Pessac, France) with one closed arm and two other arms with manually operated doors as previously^{31,32}. Briefly, two rectangular chambers (11 × 25 cm) with different cues (texture and color) are separated by a center triangular compartment (side of 11 cm) used as a neutral compartment. One pairing compartment textured black and white striped walls and floor, while the other has smooth gray floor and walls. The CPP apparatus was illuminated at 100 lux during the experiments. The first day (pretest) of the experiment, without previous habituation to the

apparatus, mice explored the environment for 900 s (15 min) and the time spent in each compartment was recorded. Conditioning was unbiased: pretest data were used to segregate the animals with equal bias so each group has an initial preference score almost null, indicating no preference on average. On day 2, 3 and 4, animals received an i.p. injection of saline (0.9%NaCl) and were immediately confined to one of the pairing chambers for 1200 s (20 min) in the morning. Groups were balanced so that animals did not all receive nicotine in the same chamber. On the afternoon of the same day mice received an injection of 0.2 mg/kg nicotine or saline and were placed in the

opposite pairing chamber. On day 5 (test), animals were allowed to freely explore the whole apparatus for 900 s (15 min). Pretest and test sessions were videorecorded and analyzed using ezTrack. The preference score is expressed in seconds and is calculated by subtracting pretest from test data. Mice were habituated to the stress of handling and injection for a minimum of one week before testing.

Brain clearing and activity mapping

Experimental design and perfusion. Mice were injected with i.p. saline or nicotine and kept in a dim, quiet room for one hour before perfusion to minimize off-target cFos expression. Mice were then perfused with 1X PBS followed by 20 mL of 4% paraformaldehyde (PFA, Electron Microscopy Services). Brains were carefully dissected from the skull, and stored in PFA overnight. Brains were stored in PBS with 0.01% Sodium Azide (Sigma-Aldrich, Germany) until clearing.

iDISCO+ whole brain immunolabeling. Whole brain clearing and immunostaining was performed following the iDISCO+ protocol previously described previously³³ with minimal modifications. All the steps of the protocol were done at room temperature with gentle shaking unless otherwise specified. All the buffers were supplemented with 0.01% Sodium Azide (Sigma-Aldrich, Germany) to prevent bacterial and fungal growth. Briefly, perfused brains were dehydrated in an increasing series of methanol (Sigma-Aldrich, France) dilutions in water (washes of 1 h in methanol 20%, 40%, 60%, 80% and 100%). An additional wash of 2 h in methanol 100% was done to remove residual water. Once dehydrated, samples were incubated overnight in a solution containing a 66% dichloromethane (Sigma-Aldrich, Germany) in methanol, and then washed twice in methanol 100% (4 h each wash). Samples were then bleached overnight at 4 °C in methanol containing a 5% of hydrogen peroxide (Sigma-Aldrich). Rehydration was done by incubating the samples in methanol 60%, 40% and 20% (1 h each wash). After methanol pretreatment, samples were washed in PBS twice 15 min and 1 h in PBS containing a 0.2% of Triton X-100 (Sigma-Aldrich) and further permeabilized by a 24 h incubation at 37 °C in Permeabilization Solution, composed by 20% dimethyl sulfoxide (Sigma-Aldrich), 2.3% Glycine (Sigma-Aldrich, USA) in PBS-T. In order to start the immunostaining, samples were first blocked with 0.2% gelatin (Sigma-Aldrich) in PBS-T for 24 h at 37 °C, the same blocking buffer was used to prepare antibody solutions. Brains were incubated with anti c-Fos primary (Synaptic systems 226-003) for 10 days at 37 °C with gentle shaking, then washed in PBS-T (twice 1 h and then overnight), and finally newly incubated for 10 days with secondary antibodies. Secondary antibodies raised in donkeys, conjugated to Alexa 647 were used (Life Technologies). After immunostaining, the samples were washed in PBS-T (twice 1 h and then overnight), dehydrated in a methanol/water increasing concentration series (20%, 40%, 60%, 80%, 100% one hour each and then methanol 100% overnight), followed by a wash in 66% dichloromethane – 33% methanol for 3 h. Methanol was washed out with two final washes in dichloromethane 100% (15 min each) and finally the samples were cleared and stored in dibenzyl ether (Sigma-Aldrich) until light sheet imaging.

Light sheet microscopy. The acquisitions were done on a LaVision Ultramicroscope II equipped with infinity-corrected objectives. The microscope was installed on an active vibration filtration device, itself put on a marble compressed-air table. Imaging was done with the following filters: 595/40 for Alexa Fluor-555, and –680/30 for Alexa Fluor-647. The microscope was equipped with the following laser lines: OBIS-561nm 100 mW, OBIS-639nm 70 mW, and used the 2nd generation LaVision beam combiner. The images were acquired with an Andor CMOS sNEO camera. Main acquisitions were done with the LVMI-Fluor 4X/O.3 WD6 LaVision Biotec objective. The microscope was connected to a computer equipped with SSD drives to speed up

the acquisition. The brain was positioned in sagittal orientation, cortex side facing the light sheet, to maximize image quality and consistency. A field of view of 1000 × 1300 pixels was cropped at the center of the camera sensor. The light sheet numerical aperture was set to NA-0.03. The 3 light sheets facing the cortex were used, while the other side illumination was deactivated to improve the axial resolution. Beam width was set to the maximum. Laser powers were set to 40–60% (639 nm). The center of the light sheet in x was carefully calibrated to the center of the field. z steps were set to 6 mm. Tile overlaps were set to 10%. The whole acquisition takes about 1 h per hemisphere. At the end of the acquisition, the objective is changed to a MI PLAN 1.1X/O.1 for the reference scan at 488 nm excitation (tissue autofluorescence). The field of view is cropped to the size of the brain, and the z-steps are set to 6 mm, and light sheet numerical aperture to 0.03 NA. It is important to crop the field of view to the size of the brain for subsequent alignment steps.

Computing resources. The data were automatically transferred every day from the acquisition computer to a Lustre server for storage. The processing with ClearMap was done on local workstations, either Dell Precision T7920 or HP Z840. Each workstation was equipped with 2 Intel Xeon Gold 6128 3.4 G 6 C/12 T CPUs, 512 Gb of 2666 MHz DDR4 RAM, 4x1Tb NVMe Class 40 Solid State Drives in a RAID0 array (plus a separate system disk), and an NVIDIA Quadro P6000, 24 Gb VRAM video card. The workstations were operated by Linux Ubuntu 20.04LTS. ClearMap 2.0 was used on Anaconda Python 3.7 environment.

ClearMap Fos+ cell counting. Tiled acquisitions of Fos-immunolabeled iDISCO+ cleared brains scanned with the light sheet microscope were processed with ClearMap 2 to generate both voxel maps of Fos cell densities, as well as region-based statistics of cell counts^{34,69}. Briefly, stitched images were processed for background removal, on which local maxima were detected to place initial seeds for the cells. A watershed was done on each seed to estimate the volume of the cell, and the cells were filtered according to their volume to exclude smaller artefactual maxima. The alignment of the brain to the Allen Brain Atlas (March 2017) was based on the acquired autofluorescence image using Elastix (<https://elastix.lumc.nl>). Filtered cell's coordinates were transformed to their reference coordinate in the Allen Brain Atlas common coordinate system⁷⁰. For voxel maps, spheres of 375 μm diameter were drawn on each filtered cell. *P* Value maps of significant differences between groups were generated using Mann–Whitney U test (SciPy implementation). Aligned voxelized datasets from each group of animals were manually inspected to identify the regional overlaps of p-value clusters, and volcano-plots of regional counts were generated.

Quantitative neuroanatomy of dopamine terminals

Tissue preparation. Mice were perfused with 1X PBS followed by 20 mL of 4% paraformaldehyde (Sigma). Brains were postfixed in PFA overnight, transferred to PBS before sectioning. Serial 50 μm thick coronal sections were made on a Leica vibratome (VTS1000) within one week of perfusion, and stored free-floating in PBS. Free-floating brain sections were then incubated for 1 h at 4 °C in a blocking solution of phosphate-buffered saline (PBS) containing 3% bovine serum albumin (BSA, Sigma; A4503) (vol/vol) and 0.2% Triton X-100 (vol/vol), and then incubated overnight at 4 °C with a sheep anti-tyrosine hydroxylase antibody (anti-TH, Milipore, Ab1542) diluted 1:500 in PBS containing 1.5% BSA and 0.2% Triton X-100. The following day, sections were rinsed with PBS, and then incubated for 3 h at room temperature with Cy3-conjugated anti-sheep secondary antibody (Jackson ImmunoResearch, 713-165-147) diluted 1:500 in a solution of 1.5% BSA in PBS. After three rinses in PBS, slices were wet-mounted using Prolong Gold Antifade Reagent (Invitrogen, P36930).

Confocal image acquisition and deconvolution. Images stacks were taken with a Confocal Laser Scanning Microscope (AI, Nikon) equipped with a 60×1.4 NA objective (oil immersion, Nikon) with pinhole aperture set to 1 Airy Unit, pixel size of 50 nm and z-step of 200 nm. Excitation wavelength and emission range for Cy-3 labeling was: ex. 561, em. 570–630. Laser intensity was set so that each image occupies the full dynamic range of the detector. Deconvolution using Maximum Likelihood Estimation algorithm was performed with Huygens software (Scientific Volume Imaging)⁷¹. 150 iterations were applied in classical mode, background intensity was averaged from the voxels with lowest intensity, and signal to noise ratio values were set to a value of 20.

Segmentation of presynaptic boutons from confocal images. Segmentation of TH+ boutons was performed in 3D in FIJI (fiji.net) using a procedure based on image analysis tools developed in the ImageJ plugin 3DImageSuite^{72–74}. First local maxima were detected. Histogram analysis and image inspection allowed the definition of a threshold intensity so that only local maxima from presynaptic objects were retained. The local maxima were then used as seeds around which 3D intensity distribution was fitted to a Gaussian curve. The intensity value which defines 95% of the area of the gauss curve was chosen as threshold for the border of the object. Buttons of similar size but different intensity are thus extracted as object of similar size. The border of the object was determined following the so-called block algorithm; starting around the local maxima, voxels which followed three criteria were included in the object (intensity above the threshold, intensity lower than previously included voxel, and the inclusion is validated if neighboring voxels are included as well). Counts were used to determine a density for the obtained image stack and normalized to a standard volume of 10 μm × 10 μm × 10 μm to make comparisons between images with different stack sizes, then exported to.csv.

In vivo electrophysiology

Mice were deeply anaesthetized with (1) an IP injection of chloral hydrate (400 mg/kg), supplemented as required to maintain optimal anesthesia throughout the experiment, or (2) isoflurane delivered continuously (5% induction, 2–3% maintenance; TEMSega). The scalp was opened and a hole was drilled in the skull above the location of the VTA. Intravenous administration of saline or nicotine (30 μg/kg) was carried out through a catheter (30 G needle connected to polyethylene tubing PE10) connected to a Hamilton syringe, into the saphenous vein of the animal. Extracellular recording electrodes were constructed from 1.5 mm outer diameter/1.17 mm inner diameter borosilicate glass tubing (Harvard Apparatus) using a vertical electrode puller (Narishige). The tip was broken straight and clean under microscopic control to obtain a diameter of about 1 μm. The electrodes were filled with a 0.5% NaCl solution containing 1.5% of neurobiotin® tracer (VECTOR laboratories) yielding impedances of 6–9 MΩ. Electrical signals were amplified by a high-impedance amplifier (Axon Instruments) and monitored audibly through an audio monitor (A.M. Systems Inc.). The signal was digitized, sampled at 25 kHz, and recorded on a computer using Spike2 software (Cambridge Electronic Design) for later analysis. The electrophysiological activity was sampled in the central region of the VTA (coordinates: between 3.1 and 4 mm posterior to bregma, 0.3 to 0.7 mm lateral to midline, and 4 to 4.8 mm below brain surface). Individual electrode tracks were separated from one another by at least 0.1 mm in the horizontal plane. Spontaneously active DA neurons were identified based on previously established electrophysiological criteria⁷⁵.

After recording, a subset of nicotine-responsive cells were labeled by electroporation of their membrane: successive currents squares were applied until the membrane breakage, to fill the cell soma with neurobiotin contained into the glass pipet⁷⁶. To be able to establish correspondence between neurons responses and their localization in

the VTA, we labeled one type of response per mouse: solely activated neurons or solely inhibited neurons, with a limited number of cells per brain (1 to 4 neurons maximum, 2 by hemisphere), always with the same concern of localization of neurons in the VTA.

Ex vivo patch-clamp recordings

Mice were anesthetized (Ketamine 150 mg/kg; Xylazine 10 mg/kg) and transcardially perfused with aCSF for slice preparation. For VTA recordings, horizontal 250 μm slices were obtained in bubbled ice-cold 95% O₂/5% CO₂ aCSF containing (in mM): KCl 2.5, NaH₂PO₄ 1.25, MgSO₄ 10, CaCl₂ 0.5, glucose 11, sucrose 234, NaHCO₃ 26. Slices were then incubated in aCSF containing (in mM): NaCl 119, KCl 2.5, NaH₂PO₄ 1.25, MgSO₄ 1.3, CaCl₂ 2.5, NaHCO₃ 26, glucose 11, at 37 °C for 1 h, and then kept at room temperature. Slices were transferred and kept at 32–34 °C in a recording chamber superfused with 2.5 ml/min aCSF. Visualized whole-cell voltage-clamp recording technique was used to measure synaptic responses using an upright microscope (Olympus France). Putative DA neurons were recorded in the lateral VTA and identified using criteria such as localization and cell body size, as well as electrophysiological signature (e.g., broad action potential, and large I_h current)⁷⁵. Spontaneous excitatory postsynaptic currents (sEPSCs) induced by puffing nicotine onto DA cells were measured, as well as analyses of paired-pulse ratios (PPR) and AMPA-R/NMDA-R ratios as an index of synaptic adaptations.

Experiments were obtained using a Multiclamp 700B (Molecular Devices, Sunnyvale, CA). Signals were collected and stored using a Digidata 1440 A converter and pCLAMP 10.2 software (Molecular Devices, CA). In all cases, analyses were performed using Clampfit 10.2 (Axon Instruments, USA) and Prism (Graphpad, USA).

Paired-pulse ratios (PPR) and AMPA-R/NMDA-R ratios were assessed in voltage-clamp mode using an internal solution containing (in mM) 130 CsCl, 4 NaCl, 2 MgCl₂, 1.1 EGTA, 5 HEPES, 2 Na₂ATP, 5 sodium creatine phosphate, 0.6 Na₃GTP, and 0.1 spermine. The PPR protocol consisted in two evoked pulses 50 ms apart applied every 15 s at V = −60 mV. Synaptic currents were evoked by stimuli (10 μs) at 0.15 Hz through a glass pipette placed 200 μm from the patched neurons. Voltage was then raised to V = +40 mV and synaptic currents were evoked in the absence and in the presence of AMPA-R antagonist DNQX as previously described for AMPA-R/NMDA-R ratios⁷⁷.

To assess NMDA currents, voltage-clamp were performed using an internal solution containing (in mM) 130 CsCl, 4 NaCl, 2 MgCl₂, 1.1 EGTA, 5 HEPES, 2 Na₂ATP, 5 sodium creatine phosphate, 0.6 Na₃GTP, and 0.1 spermine. Cells were held at +40 mV and NMDA synaptic currents were evoked 15 times (3 times per min) by stimuli of 0.1 ms every 20 s through a glass pipette placed 200 μm from the patched neurons. Stimulus position and intensity were set to achieve 30–50% of maximum response amplitude in each cell. NMDAR EPSCs were pharmacologically isolated by adding 50 μM picrotoxin (Sigma-Aldrich, dissolved in DMSO) to block GABAergic transmission and DNQX (10 μM; Sigma-Aldrich, dissolved in DMSO) to block AMPA receptors. To evaluate the contribution of GluN2B containing-NMDARs, synaptic currents were evoked during 5 min to established a baseline response and after 10 min incubation in the bath solution with Ifenprodil 5 μM (Sigma Aldrich, France). For analysis, the time courses were obtained by normalizing each recording to the average value of all points constituting the first 5 min stable baseline. For the analysis the average of the traces were calculate in presence and absence of Ifenprodil and the area under the curve (AUC) was calculated using Clampfit program. For the normalization per cell, the average of the amplitude of the currents were analyzed in presence and absence of Ifenprodil. The data represent the percentage of change in presence of Ifenprodil with respect the baseline in absence of antagonist.

For analyses of nAChR currents and nicotinic modulation of sEPSCs, nicotine was applied by a ‘puff’ with air-pressure pulses controlled by a Picospritzer III (General Valve). A drug-filled pipette was

moved within 20–40 μm from the recorded neuron and a pClamp protocol triggered a puff application of nicotine (10 mM) onto the recorded neuron with a 20–80 ms, 20-psi pressure ejection. Peak amplitude (pA) was compared between groups. Clampfit establishes whether the best fit of the traces should have 1 or 2 terms. This always corroborated visual observation. Time constants (τ values) of the decays were calculated by exponential fitting. In the cases where two phases were observed, we calculated the weighted τ (consisting of an exponential fit with two terms, one fast and one slow). This weighted time constant was calculated using the relative contribution from each of these components, applying the formula: $\tau_w = [(AF * \tau_f) + (AS * \tau_s)] / (AF + AS)$, where AF and AS are the relative amplitudes of the two exponential components, and τ_f and τ_s are the corresponding time constants. τ and τ_w were not different within the treatment groups, so they were pooled for between-groups comparison. Finally, charge transfer of nicotinic currents was calculated as the integral of the current (AUC) in the time window between onset and decay. To compare the frequency and amplitudes of sEPSCs in response to acute NIC exposure between treated animals and controls, epochs of at least 30 s were recorded before and after puff application of nicotine on VTA DA neurons. Analyses were performed using Clampfit 10.2 (Axon Instruments, USA) and Prism (Graphpad, USA).

DREADD experiments

DAT-Cre mice, in which Cre recombinase expression is restricted to DA neurons without disrupting endogenous dopamine transporter (DAT) expression⁶³, were weaned at PND 21 \pm 1 and treated with nicotine (100 $\mu\text{g}/\text{mL}$ in 2% saccharine) for one week. When they reached adulthood, they were injected with Cre-dependent (DIO) DREADD or control (tdTomato) viruses. Adult DAT-Cre mice were anesthetized with a mixture of oxygen (1L/min) and 3–4% isoflurane (Vetflurane, Virbac) for the induction of anesthesia, and then placed on a warming pad in a stereotaxic frame (David Kopf) and maintained under anesthesia throughout the surgery at 2% isoflurane. A local anesthetic (Lurocaine) was applied at the location of the scalp incision and 0.1 μL of buprenorphine (Buprecare, 1 mg/kg) was injected subcutaneously before the procedure. Mice then received bilateral injections of a retrogradely-transported inhibitory DREADD AAV (ssAAV-retro/2-hSyn1-dlox-hM4D(Gi)_mCherry(rev)-dlox-WPRE-hGHp(A), Viral Vector Facility Zurich) or control virus (ssAAV-retro/2-hEFla-dlox-dTomato-EGFP(rev)-dlox-WPRE-hGHp(A), Viral Vector Facility Zurich) into the medial NAc (bregma +1.7 mm, lateral \pm 0.45 mm, ventral $-$ 4.1 mm).

Mice were tested in the EOM 4–5 weeks after viral injections to allow full expression of the DREADD or control viruses at the level of the VTA. Clozapine-N-oxide (5 mg/kg, CNO) was injected i.p. one hour before the mice received nicotine or saline and entered into the EOM task, as described above. While CNO can have off-target effects⁷⁸, the 5 mg/kg dose used in our experiments is below the threshold identified for off-target effects. In support of this idea, we did not see any differences in saline-injected mice under CNO, regardless of their virus (DREADD or control) status.

Following the EOM, mice were perfused with 1X PBS followed by 20 mL of 4% paraformaldehyde (Sigma). Brains were postfixed in PFA overnight, and transferred to PBS before sectioning. Serial 50 μm thick coronal sections were made on a Leica vibratome (VTS1000) within one week of perfusion, and stored free-floating in PBS. Free-floating brain sections were then incubated for 1 h at 4 $^{\circ}\text{C}$ in a blocking solution of phosphate-buffered saline (PBS) containing 3% bovine serum albumin (BSA, Sigma; A4503) (vol/vol) and 0.2% Triton X-100 (vol/vol), and then incubated overnight at 4 $^{\circ}\text{C}$ with a sheep anti-tyrosine hydroxylase antibody (anti-TH, Milipore, Ab1542) diluted 1:500 in PBS containing 1.5% BSA and 0.2% Triton X-100. The following day, sections were rinsed with PBS, and then incubated for 3 h at room temperature with Cy5-conjugated anti-sheep secondary antibody (Jackson ImmunoResearch, 713-175-147) diluted 1:500 in a solution of 1.5% BSA in PBS.

After three rinses in PBS, slices were wet-mounted using Prolong Gold Antifade Reagent containing DAPI (Invitrogen, P36931). Viral expression was evaluated by observing the unamplified expression of mCherry or tdTomato via a Rhodamine filter on an epifluorescent microscope (Zeiss Axio Imager), dopamine neurons were identified by TH staining via a Cy5 filter, and non-dopamine cell bodies were evaluated by DAPI staining. All neurons expressing the DREADD or control viruses co-expressed TH, and staining was limited to the medial VTA in line with previous reports on the location of neurons projecting to the medial NAc⁷⁹.

Statistical analysis

All statistical analysis and graphs were made using R, a language and environment for statistical computing (Team, 2005, <http://www.r-project.org>), with the exception of in vitro electrophysiology data, which was analyzed in Prism (GraphPad). Data from behavioral experiments was exported from acquisition software (TSE system) or from ezTrack video tracking as a.csv file, and read directly into R. Quantifications from ClearMap or from bouton analysis in Fiji were likewise exported as.csv files and read directly into R. CSV files of cell counts by region were imported into R from ClearMap. Correlations and clustering were then performed in R using the {stats} package, and networks were created {igraph} package. For the measurement of neuronal activity in single-unit recordings, timestamps of action potentials were extracted in Spike 2, analyzed in R, and expressed as the average firing frequency (in Hz) and the percentage of spikes-within-burst (%SWB = number of spikes within burst divided by total number of spikes in a given window). Neuronal basal activity was defined on recordings of a minimum of three minutes. Firing frequency was quantified on overlapping 60-second windows shifted by 15-s time steps. For each neuron, the firing frequency was rescaled as a percentage of its baseline value averaged during 3 min before nicotine injection. The responses to nicotine are thus presented as a percentage of variation from baseline (mean \pm S.E.M.). The effect of nicotine was assessed by comparison of the maximum of firing frequency variation induced by nicotine and saline injection. For activated (respectively inhibited) neurons, the maximal (respectively minimal) value of the firing frequency was measured within the response period (3 min) that followed nicotine or saline injection. The results are presented as mean \pm S.E.M. of the difference of maximum variation after nicotine or saline.

Reporting summary

Further information on research design is available in the Nature Portfolio Reporting Summary linked to this article.

Data availability

Source data are provided with this paper. In addition, the data generated in this study have been deposited in the Zenodo database under <https://doi.org/10.5281/zenodo.13684023> (<https://zenodo.org/uploads/13684023>). Source data are provided with this paper.

Code availability

Graphs and statistical analyses were generated using standard code written in R (version 4.4.1). All codes used to run the analysis are available from the authors upon request.

References

- Ezzati, M. et al. Selected major risk factors and global and regional burden of disease. *Lancet* **360**, 1347–1360 (2002).
- Substance Abuse and Mental Health Services Administration, Results from the 2011 National Survey on Drug Use and Health: Summary of National Findings, NSDUH Series H-44, HHS Publication No. (SMA) 12-4713. Rockville, MD: Substance Abuse and Mental Health Services Administration (2012).

3. Anthony, J. C. & Petronis, K. R. Early-onset drug use and risk of later drug problems. *Drug Alcohol Depend.* **40**, 9–15 (1995).
4. Grant, B. F. Age at smoking onset and its association with alcohol consumption and DSM-IV alcohol abuse and dependence: results from the national longitudinal alcohol epidemiologic survey. *J. Subst. Abuse.* **10**, 59–73 (1998).
5. Jamal, M., Does, A. J. W. Vd, Penninx, B. W. J. H. & Cuijpers, P. Age at smoking onset and the onset of depression and anxiety disorders. *Nicotine Tob. Res.* **13**, 809–819 (2011).
6. Choi, W. S., Patten, C. A., Gillin, J. C., Kaplan, R. M. & Pierce, J. P. Cigarette smoking predicts development of depressive symptoms among U.S. Adolescents. *Ann. Behav. Med.* **19**, 42–50 (1997).
7. Leslie, F. M. Unique, long-term effects of nicotine on adolescent brain. *Pharmacol. Biochem. Behav.* **173**, 1016. <https://doi.org/10.1016/j.pbb.2020.173010> (2020).
8. Ren, M., Lotfipour, S. & Leslie, F. Unique effects of nicotine across the lifespan. *Pharmacol. Biochem. Behav.* **214**, 173343 (2022).
9. Barth, B., Portella, A. K., Dubé, L., Meaney, M. J. & Silveira, P. P. Early life origins of ageing and longevity. in *Early Life Origins of Ageing and Longevity* 121–140. https://doi.org/10.1007/978-3-030-24958-8_7 (2019).
10. Reynolds, L. M. & Flores, C. Adolescent dopamine development: connecting experience with vulnerability or resilience to psychiatric disease. in *Diagnosis, Management and Modeling of Neurodevelopmental Disorders* (eds. Martin, C. R., Preedy, V. R. & Rajendram, R.) (Academic Press, 2021). <https://doi.org/10.1016/b978-0-12-817988-8.00026-9>.
11. Reynolds, L. M. & Flores, C. Mesocorticolimbic dopamine pathways across adolescence: diversity in development. *Front. Neural Circuit.* **15**, 735625 (2021).
12. Changeux, J.-P. Nicotine addiction and nicotinic receptors: lessons from genetically modified mice. *Nat. Rev. Neurosci.* **11**, 389–401 (2010).
13. Morel, C., Montgomery, S. & Han, M.-H. Nicotine and alcohol: the role of midbrain dopaminergic neurons in drug reinforcement. *Eur. J. Neurosci.* **114**, 13012 (2018).
14. Faure, P., Tolu, S., Valverde, S. & Naudé, J. Role of nicotinic acetylcholine receptors in regulating dopamine neuron activity. *Neuroscience* **282**, 86–100 (2014).
15. Wills, L. et al. Neurobiological mechanisms of nicotine reward and aversion. *Pharmacol. Rev.* **74**, 271–310 (2022).
16. Placzek, A. N., Zhang, T. A. & Dani, J. A. Age dependent nicotinic influences over dopamine neuron synaptic plasticity. *Biochem Pharm.* **78**, 686–692 (2009).
17. Jobson, C. L. M. et al. Adolescent nicotine exposure induces dysregulation of mesocorticolimbic activity states and depressive and anxiety-like prefrontal cortical molecular phenotypes persisting into adulthood. *Cereb. Cortex* **29**, 3140–3153 (2018).
18. Phillips, R. A. et al. An atlas of transcriptionally defined cell populations in the rat ventral tegmental area. *Cell Rep.* **39**, 110616 (2022).
19. Poulin, J.-F. et al. Mapping projections of molecularly defined dopamine neuron subtypes using intersectional genetic approaches. *Nat. Neurosci.* **21**, 1 (2018).
20. Margolis, E. B., Hjelmstad, G. O., Fujita, W. & Fields, H. L. Direct bidirectional μ -Opioid control of midbrain dopamine neurons. *J. Neurosci.* **34**, 14707–14716 (2014).
21. Juarez, B. & Han, M.-H. Diversity of dopaminergic neural circuits in response to drug exposure. *Neuropsychopharmacol.* **41**, 2424–2446 (2016).
22. Lammel, S., Lim, B. K. & Malenka, R. C. Reward and aversion in a heterogeneous midbrain dopamine system. *Neuropharmacology* **76**, 351–359 (2014).
23. Nguyen, C. et al. Nicotine inhibits the VTA-to-amygdala dopamine pathway to promote anxiety. *Neuron* <https://doi.org/10.1016/j.neuron.2021.06.013> (2021).
24. Morel, C. et al. Midbrain projection to the basolateral amygdala encodes anxiety-like but not depression-like behaviors. *Nat. Commun.* **13**, 1532 (2022).
25. Reynolds, L. M. et al. Amphetamine disrupts dopamine axon growth in adolescence by a sex-specific mechanism in mice. *Nat. Commun.* **14**, 4035 (2023).
26. Glantz, S., Jeffers, A. & Winickoff, J. P. Nicotine addiction and intensity of e-Cigarette use by adolescents in the US, 2014 to 2021. *Jama Netw. Open* **5**, e2240671 (2022).
27. Riggs, N., Chou, C.-P., Li, C. & Pentz, M. A. Adolescent to emerging adulthood smoking trajectories: When do smoking trajectories diverge, and do they predict early adulthood nicotine dependence? *Nicotine Tob. Res.* **9**, 1147–1154 (2007).
28. Fowler, C. D. & Kenny, P. J. Intravenous nicotine self-administration and cue-induced reinstatement in mice: effects of nicotine dose, rate of drug infusion and prior instrumental training. *Neuropharmacology* **61**, 687–698 (2011).
29. Mondoloni, S. et al. Prolonged nicotine exposure reduces aversion to the drug in mice by altering nicotinic transmission in the interpeduncular nucleus. *eLife* **12**, e80767 (2023).
30. Fowler, C. D., Lu, Q., Johnson, P. M., Marks, M. J. & Kenny, P. J. Habenular $\alpha 5$ nicotinic receptor subunit signalling controls nicotine intake. *Nature* **471**, 597–601 (2011).
31. Cuttoli, R. D. et al. Manipulating midbrain dopamine neurons and reward-related behaviors with light-controllable nicotinic acetylcholine receptors. *Elife* **7**, e37487 (2018).
32. Jehl, J. et al. The interpeduncular nucleus blunts the rewarding effect of nicotine. *bioRxiv* 2023.10.05.561018 <https://doi.org/10.1101/2023.10.05.561018> (2023).
33. Renier, N. et al. iDISCO: a simple, rapid method to immunolabel large tissue samples for volume imaging. *Cell* **159**, 896–910 (2014).
34. Renier, N. et al. Mapping of brain activity by automated volume analysis of immediate early genes. *Cell* **165**, 1789–1802 (2016).
35. Hale, M. W. et al. Exposure to an open-field arena increases c-Fos expression in a distributed anxiety-related system projecting to the basolateral amygdaloid complex. *Neuroscience* **155**, 659–672 (2008).
36. Singewald, N., Salchner, P. & Sharp, T. Induction of c-Fos expression in specific areas of the fear circuitry in rat forebrain by anxiogenic drugs. *Biol. Psychiat.* **53**, 275–283 (2003).
37. Singewald, N. & Sharp, T. Neuroanatomical targets of anxiogenic drugs in the hindbrain as revealed by Fos immunocytochemistry. *Neuroscience* **98**, 759–770 (2000).
38. Pich, E. M., Chiamulera, C. & Tessari, M. Neural substrate of nicotine addiction as defined by functional brain maps of gene expression. *J. Physiol.-Paris* **92**, 225–228 (1998).
39. Pagliusi, S. R., Tessari, M., DeVevey, S., Chiamulera, C. & Pich, E. M. The reinforcing properties of nicotine are associated with a specific patterning of c-fos expression in the rat brain. *Eur. J. Neurosci.* **8**, 2247–2256 (1996).
40. Bullmore, E. & Sporns, O. Complex brain networks: graph theoretical analysis of structural and functional systems. *Nat. Rev. Neurosci.* **10**, 186–198 (2009).
41. Bellone, C., Mamei, M. & Lüscher, C. In utero exposure to cocaine delays postnatal synaptic maturation of glutamatergic transmission in the VTA. *Nat. Neurosci.* **14**, 1446 (2011).
42. Bellone, C. & Nicoll, R. A. Rapid bidirectional switching of synaptic NMDA receptors. *Neuron* **55**, 779–785 (2007).

43. Lammel, S., Ion, D. I., Roeper, J. & Malenka, R. C. Projection-specific modulation of dopamine neuron synapses by aversive and rewarding stimuli. *Neuron* **70**, 855–862 (2011).
44. Basilico, B. et al. Microglia shape presynaptic properties at developing glutamatergic synapses. *Glia* **67**, 53–67 (2019).
45. Kota, D., Martin, B. R., Robinson, S. E. & Damaj, M. I. Nicotine dependence and reward differ between adolescent and adult male mice. *J. Pharmacol. Exp. Ther.* **322**, 399–407 (2007).
46. Kota, D., Martin, B. R. & Damaj, M. I. Age-dependent differences in nicotine reward and withdrawal in female mice. *Psychopharmacology* **198**, 201–210 (2008).
47. Vastola, B. J., Douglas, L. A., Varlinskaya, E. I. & Spear, L. P. Nicotine-induced conditioned place preference in adolescent and adult rats. *Physiol. Behav.* **77**, 107–114 (2002).
48. Elliott, B. M., Faraday, M. M., Phillips, J. M. & Grunberg, N. E. Effects of nicotine on elevated plus maze and locomotor activity in male and female adolescent and adult rats. *Pharmacol. Biochem. Behav.* **77**, 21–28 (2004).
49. Bariselli, S. et al. Role of VTA dopamine neurons and neuroligin 3 in sociability traits related to nonfamiliar conspecific interaction. *Nat. Commun.* **9**, 3173 (2018).
50. Miech, R., Johnston, L., O'Malley, P. M., Bachman, J. G. & Patrick, M. E. Adolescent Vaping and Nicotine Use in 2017–2018 - U.S. National Estimates. *N. Engl. J. Med.* **380**, 192–193 (2019).
51. Beier, K. T. et al. Circuit architecture of VTA dopamine neurons revealed by systematic input-output mapping. *Cell* **162**, 622–634 (2015).
52. Ford, C. P., Mark, G. P. & Williams, J. T. Properties and opioid inhibition of mesolimbic dopamine neurons vary according to target location. *J. Neurosci.* **26**, 2788–2797 (2006).
53. Mejias-Aponte, C. A., Ye, C., Bonci, A., Kiyatkin, E. A. & Morales, M. A subpopulation of neurochemically-identified ventral tegmental area dopamine neurons is excited by intravenous cocaine. *J. Neurosci.* **35**, 1965–1978 (2015).
54. Lin, W. C. et al. Transient food insecurity during the juvenile-adolescent period affects adult weight, cognitive flexibility, and dopamine neurobiology. *Curr. Biol.* **32**, 3690–3703.e5 (2022).
55. Wills, L. & Kenny, P. J. Addiction-related neuroadaptations following chronic nicotine exposure. *J Neurochem* <https://doi.org/10.1111/jnc.15356> (2021).
56. Fowler, C. D. & Kenny, P. J. Nicotine aversion: neurobiological mechanisms and relevance to tobacco dependence vulnerability. *Neuropharmacology* **76**, 533–544 (2014).
57. Lavolette, S. R. & Kooy, Dvander The neurobiology of nicotine addiction: bridging the gap from molecules to behaviour. *Nat. Rev. Neurosci.* **5**, 55–65 (2004).
58. Reynolds, L. M. et al. Early adolescence is a critical period for the maturation of inhibitory behavior. *Cereb. Cortex* **29**, 3676–3686 (2019).
59. Cross, S. J., Linker, K. E. & Leslie, F. M. Sex-dependent effects of nicotine on the developing brain. *J. Neurosci. Res.* **95**, 422–436 (2017).
60. Okoli, C., Greaves, L. & Fagyas, V. Sex differences in smoking initiation among children and adolescents. *Public Health* **127**, 3–10 (2013).
61. Duan, Z., Wang, Y. & Huang, J. Sex difference in the association between electronic cigarette use and subsequent cigarette smoking among U.S. adolescents: findings from the PATH study waves 1–4. *Int. J. Environ. Res. Public Health* **18**, 1695 (2021).
62. Allain, F., Minogianis, E.-A., Roberts, D. C. S. & Samaha, A.-N. How fast and how often: the pharmacokinetics of drug use are decisive in addiction. *Neurosci. Biobehav. Rev.* **56**, 166–179 (2015).
63. Turiault, M. et al. Analysis of dopamine transporter gene expression pattern – generation of DAT-iCre transgenic mice. *Febs J.* **274**, 3568–3577 (2007).
64. Klein, L. C., Stine, M. M., Vandenberg, D. J., Whetzel, C. A. & Kamens, H. M. Sex differences in voluntary oral nicotine consumption by adolescent mice: a dose-response experiment. *Pharm. Biochem. Be* **78**, 13–25 (2004).
65. Nesil, T., Kanit, L., Collins, A. C. & Pogun, S. Individual differences in oral nicotine intake in rats. *Neuropharmacology* **61**, 189–201 (2011).
66. Locklear, L. L., McDonald, C. G., Smith, R. F. & Fryxell, K. J. Adult mice voluntarily progress to nicotine dependence in an oral self-selection assay. *Neuropharmacology* **63**, 582–592 (2012).
67. Bagdas, D. et al. Assessing nicotine dependence using an oral nicotine free-choice paradigm in mice. *Neuropharmacology* **157**, 107669 (2019).
68. Pennington, Z. T. et al. ezTrack: an open-source video analysis pipeline for the investigation of animal behavior. *Sci. Rep.* **9**, 19979 (2019).
69. Kirst, C. et al. Mapping the fine-scale organization and plasticity of the brain vasculature. *Cell* **180**, 780–795.e25 (2020).
70. Wang, Q. et al. The allen mouse brain common coordinate framework: a 3D reference Atlas. *Cell* **181**, 936–953.e20 (2020).
71. Heck, N., Betuing, S., Vanhoutte, P. & Caboche, J. A deconvolution method to improve automated 3D-analysis of dendritic spines: application to a mouse model of Huntington's disease. *Brain Struct. Funct.* **217**, 421–434 (2011).
72. Heck, N. et al. A new automated 3D detection of synaptic contacts reveals the formation of cortico-striatal synapses upon cocaine treatment in vivo. *Brain Struct. Funct.* **220**, 2953–2966 (2015).
73. Gilles, J.-F., Santos, M. D., Boudier, T., Bolte, S. & Heck, N. DiAna, an ImageJ tool for object-based 3D co-localization and distance analysis. *Methods* **115**, 55–64 (2017).
74. Santos, M. D. et al. Cocaine increases dopaminergic connectivity in the nucleus accumbens. *Brain Struct. Funct.* **104**, 1–11 (2017).
75. Ungless, M. A. & Grace, A. A. Are you or aren't you? Challenges associated with physiologically identifying dopamine neurons. *Trends Neurosci.* **35**, 422–430 (2012).
76. Pinault, D. A novel single-cell staining procedure performed in vivo under electrophysiological control: morpho-functional features of juxtacellularly labeled thalamic cells and other central neurons with biocytin or Neurobiotin. *J. Neurosci. Meth.* **65**, 113–136 (1996).
77. Morel, C. et al. Nicotinic receptors mediate stress-nicotine detrimental interplay via dopamine cells' activity. *Mol. Psychiatr.* **36**, 1418 (2017).
78. Manvich, D. F. et al. The DREADD agonist clozapine N-oxide (CNO) is reverse-metabolized to clozapine and produces clozapine-like interoceptive stimulus effects in rats and mice. *Sci. Rep.* **8**, 3840 (2018).
79. Lammel, S. et al. Unique properties of mesoprefrontal neurons within a dual mesocorticolimbic dopamine system. *Neuron* **57**, 760–773 (2008).

Acknowledgements

This work was supported by the Centre National de la Recherche Scientifique CNRS UMR 8246, INSERM U1130, the Foundation for Medical Research (FRM, Equipe FRM DEQ2013326488 to P.F.; Equipe FRM EQU202403018036 to J.B.), the French National Cancer Institute (Grant TABAC-16-022, TABAC-19-020 and SPA-21-002 to P.F.), and French state funds managed by the ANR (ANR-20 NICADO to P.F. and J.B., ANR-19-CE16-0028 Bavar to P.F. and N.R.). The project was also supported by the French government through the France 2030 investment plan managed by the National Research Agency (ANR), as part of the Initiative of Excellence of Université Côte d'Azur under reference number ANR-15-IDEX-01 and The Collegium of Advanced Studies to J.B. LMR was supported by a NIDA–Inserm Postdoctoral Drug Abuse Research Fellowship. C.N. was supported by a fourth-year PhD fellowship from the Biopsy Labex. We are grateful for support from the animal facilities (IBPS) and Otilia de Oliveira, Noemie Karakaplan-Dherbe and Emilie Tubeuf at ESPCI animal facilities.

Author contributions

L.M.R. and P.F. designed the study. L.M.R., A.G., and C.F. performed the behavioral experiments. L.M.R., T.T., and DRajot performed iDISCO and ClearMap experiments with support from N.R. R.C.C., DRigoni and S.P.F. performed ex vivo electrophysiological recordings with support from J.B. L.M.R., S.L.F., C.N., T.L.B., and F.M. performed in vivo electrophysiological recordings. L.M.R. performed the surgeries and virus injections. L.M.R. and A.G. performed quantitative neuroanatomy experiments with support from N.H. L.M.R., A.G., R.C.C., DRigoni, T.T., J.B., and P.F. analyzed the data. L.M.R. wrote the paper with inputs from A.M., F.M., J.B., and P.F. All authors read and edited the manuscript. N.R., J.B., and P.F. secured the funding.

Competing interests

The authors declare no competing interests.

Additional information

Supplementary information The online version contains supplementary material available at <https://doi.org/10.1038/s41467-024-53327-w>.

Correspondence and requests for materials should be addressed to Lauren M. Reynolds or Philippe Faure.

Peer review information *Nature Communications* thanks the anonymous reviewers for their contribution to the peer review of this work. A peer review file is available.

Reprints and permissions information is available at <http://www.nature.com/reprints>

Publisher's note Springer Nature remains neutral with regard to jurisdictional claims in published maps and institutional affiliations.

Open Access This article is licensed under a Creative Commons Attribution 4.0 International License, which permits use, sharing, adaptation, distribution and reproduction in any medium or format, as long as you give appropriate credit to the original author(s) and the source, provide a link to the Creative Commons licence, and indicate if changes were made. The images or other third party material in this article are included in the article's Creative Commons licence, unless indicated otherwise in a credit line to the material. If material is not included in the article's Creative Commons licence and your intended use is not permitted by statutory regulation or exceeds the permitted use, you will need to obtain permission directly from the copyright holder. To view a copy of this licence, visit <http://creativecommons.org/licenses/by/4.0/>.

© The Author(s) 2024